Advanced Review

Dirac-exact relativistic methods: the normalized elimination of the small component method†

Dieter Cremer,* Wenli Zou and Michael Filatov

Dirac-exact relativistic methods, i.e., 2- or 1-component methods which exactly reproduce the one-electron energies of the original 4-component Dirac method, have established a standard for reliable relativistic quantum chemical calculations targeting medium- and large-sized molecules. Their development was initiated and facilitated in the late 1990s by Dyall's development of the normalized elimination of the small component (NESC). Dyall's work has fostered the conversion of NESC and related (later developed) methods into routinely used, multipurpose Dirac-exact methods by which energies, first-order, and second-order properties can be calculated at computational costs, which are only slightly higher than those of nonrelativistic methods. This review summarizes the development of a generally applicable 1-component NESC algorithm leading to the calculation of reliable energies, geometries, electron density distributions, electric moments, electric field gradients, hyperfine structure constants, contact densities and Mössbauer isomer shifts, nuclear quadrupole coupling constants, vibrational frequencies, infrared intensities, and static electric dipole polarizabilities. In addition, the derivation and computational possibilities of 2-component NESC methods are discussed and their use for the calculation of spin-orbit coupling (SOC) effects in connection with spin-orbit splittings and SOC-corrected energies are demonstrated. The impact of scalar relativistic and spin-orbit effects on molecular properties is presented.

How to cite this article:
WIREs Comput Mol Sci 2014, 4:436–467. doi: 10.1002/wcms.1181

IMPORTANCE OF RELATIVISTIC EFFECTS IN CHEMISTRY

The identification and understanding of relativistic effects is essential for an expert analysis of the chemistry of heavy and superheavy elements.[1–15] For a long time, relativistic effects were not considered to be important for chemistry because chemical processes and chemical properties are largely determined by the valence electrons of an atom. This belief was based on a misleading interpretation of the so-called *mass-velocity effect* originally discovered by Einstein[16] when developing the theory of special relativity:

$$m_e = \frac{m_0}{\sqrt{1-(v/c)^2}} = \frac{m_0}{\sqrt{1-\beta^2}} \qquad (1)$$

According to the mass-velocity effect, the mass of an electron at rest, m_0, increases with its velocity v to the effective mass m_e ($c = 137.035\ 999\ 074(44)$ atomic units: speed of light[17]) and this will lead to a decrease of the Bohr radius r_B of an electron because the latter is proportional to $1/m_e$.[18] The shortening of the Bohr radius of an electron orbit leads to an increase of nucleus–electron attraction and relates in the quantum mechanical description to a contraction of the 1s-orbital.

Using the virial theorem $E = -T$ (the total energy of an atom or molecule is equal to the negative

*Correspondence to: dcremer@smu.edu

Computational and Theoretical Chemistry Group (CATCO), Department of Chemistry, Southern Methodist University, Dallas, TX, USA

†This article is dedicated to Kenneth G. Dyall

Conflict of interest: The authors have declared no conflicts of interest for this article.

of its kinetic energy), the ground state energy of a hydrogen-like ion with atomic number Z can be expressed according to

$$-\frac{1}{2}Z^2 = -\frac{1}{2}v^2 \tag{2}$$

where atomic units are used. Hence, $v^2 = Z^2$ follows and by this the ratio $\beta = v/c = Z/c$ can be predicted to adopt significant values only for the 1s-electrons of heavy atoms (large Z). Following this argument, the general expectation was that only for the 1s electrons of atoms with $Z \geq 80$ does the mass-velocity become important, and therefore relativity is a physics rather than a chemistry problem.

However, this interpretation of the mass-velocity effect overlooked the fact that the higher s-orbital states including the valence s-orbital also show strong relativistic effects according to the exact solution of the Dirac equation. Often this is explained in a rather simplified way that the s-orbitals with principal quantum number $n > 1$ have to be orthogonal to the contracted 1s-orbital, which leads to a propagation of the orbital contraction into the valence shell and by this becomes chemically relevant. The contracted orbitals adopt lower energies compared to the nonrelativistic situation and this has far-reaching consequences for the chemistry of the corresponding atom.

Besides the contraction of the s-orbitals, there is also a (smaller) contraction of the p-orbitals because their relativistic counterparts have a finite amplitude at the position of the nuclei. Specifically, this is true for the $p_{1/2}$ spinor (for the counterpart of the nonrelativistic or scalar relativistic spin-orbital, see below) that experiences comparable relativistic effects as the $s_{1/2}$ spinor, at least for H-like systems. The contraction of the s- and p-orbitals leads to a second, generally observed, relativistic effect: the nuclei are more shielded by the s- and p-electron density so that the electron–nucleus attraction of the d- and f-electrons is reduced; their energies are increased; their orbitals expanded; and the d- and f-densities become more diffuse than in the nonrelativistic case.

The relativistic changes in the orbital energies are reflected by the electron configurations of the transition metal atoms. For example, molybdenum prefers a [Kr] $4d^5 5s^1$ electron configuration, whereas tungsten a [Xe] $5d^4 6s^2$ configuration, thus reflecting the lowering of the energy of the 6s orbital and the increase of the 5d-orbital energy due to relativity. Similar changes are found for the pairs Nb–Ta, Ru–Os, Rh–Ir, and Pd–Pt, for which the element with the higher atomic number and the stronger relativistic effects has a higher s-orbital occupation in its ground state.[19,20]

The mass-velocity effect leads to a bond shortening, for which it seems logical to relate this effect to the relativistic orbital contraction. Extended relativistic studies, however, have clarified that these are independent phenomena because the bond contraction is due to a kinetic energy decrease in the bonding region as a result of the relativistic effects.[21–23]

The contraction of s- or p-orbitals and the expansion of d- or f-orbitals are the result of *scalar relativistic* effects. A third, nonscalar relativistic effect is spin-orbit coupling (SOC), i.e., electrons with the angular momentum quantum number $l > 0$ (p, d, f, ...) are described by spinors that are eigenfunctions of $\hat{j}^2$ and j_z where $\hat{j}$, defined by the relationships $\mathbf{j} = \mathbf{l} + \mathbf{s}$ and $\hat{j}^2 = \hat{l}^2 + \hat{s}^2 + 2\mathbf{l}\cdot\mathbf{s}$, is the total angular momentum operator ($\hat{l}$ and $\mathbf{l}$: orbital angular momentum operator and corresponding vector; $\hat{s}$ and $\mathbf{s}$: spin angular momentum operator and corresponding vector). Hence, the total angular momentum quantum number of a spinor is $j = l \pm 1/2$ thus leading to the well-known splitting of s, p, d, ... levels into $s_{1/2}$, $p_{1/2}$, $p_{3/2}$, $d_{3/2}$, $d_{5/2}$, ... levels. The splitting caused by SOC increases with the atomic number and adopts values as large as 1 eV, for example in the energy difference $E(^2P_{3/2}) - E(^2P_{1/2})$ of Tl (for a discussion of SOC, see Refs 10 and 24).

Scalar relativistic and SOC effects influence literally all physical and chemical properties of *relativistic* elements (i.e., elements from the fifth period on in the periodic table) and molecules containing these atoms. For example, relativistic effects influence the value of ionization potentials and electron affinities. Excitation spectra of molecules with heavier atoms are characteristically changed. The yellow color of gold is directly related to a relativistic decrease of the $5d - 6s$ orbital energy gap.[25] The relativistic effects on the optical properties of gold were recently reconsidered and quantified.[26,27] The relativistic bond contraction leads to a change in bond strength where bond shortening is often accompanied by a weakening of the bond.[28,29] This in turn causes changes in molecular stability and reactivity. Hence, all aspects of the chemical behavior of molecules containing relativistic atoms are changed due to scalar and/or SOC relativistic effects.

Relativistic effects are especially strong for gold (*Au-maximum* of relativity in period 6) and the neighboring elements platinum and mercury. In period 7, the maximum of relativistic effects is shifted to eka-mercury (copernicium, $Z = 112$). This becomes obvious when calculating the relativistic contraction of the 6s and 7s shell for periods 6 and 7.[30,31]

In this connection it is interesting that also the liquid state of elemental mercury is directly influenced by relativistic effects. The $6s-6p$ gap is increased by the mass-velocity effect thus effectively reducing the p-orbital (spinor) participation in bonding as well as the strength of the van der Waals interactions between Hg atoms. The latter effect is the cause for the liquid state of Hg. The peculiar properties of Hg, which are different from those of Zn and Cd, are convincing manifestations of relativity. Recently, a detailed discussion of this topic was given by Calvo et al.[32]

There are other relativistic effects such as the Lamb shift in the spectrum of the H atom,[33] which can no longer be explained using the theory of special relativity as it presents an interaction of the H electron with the vacuum. Instead, the Lamb shift requires a theoretical description employing the theory of quantum electrodynamics (QED) developed by Schwinger et al.. QED provides the theoretical basis for special relativity and thereby the description of relativistic effects in chemistry.[34] However, QED effects (Lamb shift, vacuum polarization, etc.) are very small (1% of the Dirac description of the relativistic effects for the ns binding energies of ns^1 atomic states with $Z > 41$) and therefore they are of little interest in chemistry.[35,36]

SHORT HISTORICAL OVERVIEW OF RELATIVISTIC METHODS

From the 1970s on, an increasing number of quantum chemical investigations pointed out the importance of relativity for heavy-atom chemistry. In this connection the pioneering work of Desclaux (Grenoble), Grant (Cambridge), and Pyykkö (Helsinki) has to be mentioned. The work of these theoreticians and that of many others, which followed in the last 40 years, is summarized in textbooks, review articles, and the references cited therein.[1–15] In this time span, relativistic quantum chemical methods were developed which made a reliable calculation of relativistic effects for atoms and molecules possible. A way of describing these developments is by referring to the relativistic Hamiltonian (i.e., the energy operator) used by quantum chemists.

The Dirac (D) Hamiltonian[37,38] includes Einstein's mass velocity effect in its Lorentz invariant and quantized form and the corresponding eigenvalue equation for an H-like ion leads to eigenfunctions in the form of 4-component vectors, which are called bi-spinors, that is functions comprising two spinors (2-component vectors) with the latter being the relativistic counterparts of the nonrelativistic spin orbitals. The Dirac-Coulomb (DC) Hamiltonian contains a fully relativistic one-electron part as given by the D-Hamiltonian combined with the nonrelativistic Coulomb potential, $1/r_{12}$, in the two-electron part,[39,40] thus neglecting some subtle relativistic corrections to the electron–electron interaction.[1]

The relativistic correction of the two-electron part of the Hamiltonian was first derived by Breit using perturbational procedures.[41] It contains, besides the nonrelativistic Coulomb term, two relativistic corrections where the former represents a current–current interaction and the latter represents a gage term originating from choosing a specific gage (Coulomb gage) for electron–electron interactions.[1] Although the Coulomb-Breit electron–electron interaction is not fully Lorentz invariant (correct to the order of $O(c^{-2})$), it represents a sufficiently accurate approximation to the interaction between electrons moving with relatively low velocities. The Dirac–Coulomb–Breit (DCB) Hamiltonian requires however a large load of additional calculations for the determination of the two-electron part. The DCB-Hamiltonian written in the presence of an external field includes as relativistic corrections orbit–orbit, spin-other orbit, dipole spin–spin, contact spin–spin, and the two electron Darwin interaction, of which especially the latter term may become important. In general, one can say that the two-electron relativistic corrections are rather small (with the exclusion of superheavy elements) and therefore chemically relevant results can be obtained with the DC-Hamiltonian.

Dirac-Coulomb Hartree-Fock, or Dirac-Hartree-Fock (DHF) for brevity, calculations of large molecules become expensive because they require a 4-component description of the wave function (split up into a *large* and a *small* component each with α- and β-spin part) and lead to positive eigenvalues for electrons and negative ones (shifted by the amount $-2mc^2$) for positrons (see Figure 1). The coupling between the positive and negative eigenstates leads to the small component and therefore is a direct reflection of the positronic eigenstates. The large component converges for $c \to \infty$ to the nonrelativistic electronic wave function. The terms, small and large component, result from the fact that the amplitudes of the former are much smaller than those of the latter, as seen by

$$\Psi^S \approx \frac{Z}{2mc}\Psi^L \tag{3}$$

In the case of one-electron atoms, the hydrogen wave function, $\Psi^L \approx \exp(-Zr)$ can be used. One of the

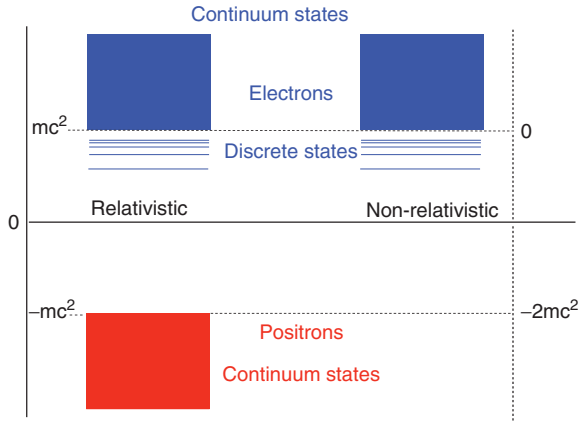

FIGURE 1 | Schematic illustration of positive and negative eigenvalues obtained by DHF calculations. Besides the discrete electronic energy levels for bound states, there is a negative (positronic) and positive (electronic) continuum at $-mc^2$ and $+mc^2$, respectively (left side). To simplify a comparison with nonrelativistic calculations, the rest mass of the electron is subtracted in the D-Hamiltonian, which corresponds to a shift by mc^2 so that the discrete electron energies become negative (right side).

effects of the small component is that the relativistic spinors differ significantly from the nonrelativistic spin-orbitals as they do not have nodal surfaces.

Since the DHF equations are solved for both the electronic and the positronic eigenstates, the energy of the former no longer corresponds to a global minimum. Numerical problems in the form of variational or inverse variational collapse may occur. The D-Hamiltonian[37,38] is not bounded from below, and therefore a variational procedure of a 4-component wave function can lead to a variational collapse, i.e., $E \rightarrow -\infty$. In atomic calculations at the single-configuration DHF level using numerical methods for the radial functions,[2,30] no particular problems arise. The boundary conditions at the origin and at infinity keep the solutions electron-like. As soon as electron correlation is introduced, e.g., by employing a multiconfigurational DHF approach, projection operators onto the electronic states have to be used to avoid dissolution into the negative energy-continuum. At the DHF level, provided that the prerequisites of the *kinetic balance* are fulfilled, a boundary can be established via the nonrelativistic energy and the first-order relativistic perturbation correction to the energy evaluated with the large-component wave function.[1] This implies the use of a *kinetically balanced* basis set[42,43] where the small-component basis functions must be chosen according to the requirement (4)

$$\chi_\mu^{\mathrm{S}} = \frac{(\boldsymbol{\sigma}\cdot\mathbf{p})}{2mc}\chi_\mu^{\mathrm{L}} \qquad (4)$$

Here, $\boldsymbol{\sigma}$ collects the Pauli matrices and $\mathbf{p}$ is the linear momentum vector. The *kinetic balance* condition (4) guarantees that the kinetic energy is properly described in the nonrelativistic limit.[42,43] The momentum operator $\mathbf{p}$ on the right side of Eq. (4) implies that the small component basis set must contain functions which are derivatives of the large-component basis functions. Basis sets which do not fulfill the kinetic balance condition can lead in a variational DHF calculation to energies below the boundary condition and thereby to a variational collapse.

Another problem of the DHF method is that with the use of finite basis sets, positronic eigenvalues significantly above the limit $-2mc^2$ can be obtained, thus causing an inverse variational collapse and an unreliable total energy.[44,45] Contrary to variational collapse, which has to do with the kinetic balance problem, inverse variational collapse results from the finite precision of computer algorithms in the case of basis functions that are very steep in the vicinity of a nucleus. This problem can be solved by increasing the precision of computer algorithms.[44] Apart from these problems, it is typical of relativistic descriptions that they require more often (than nonrelativistic ones) a multireference treatment, which is a result of SOC included into the DC-Hamiltonian.

Hence, solving the DHF equations (or similarly the Dirac-Kohn-Sham equations of relativistic density functional theory (DFT)) leads to a number of computational problems, which are enhanced by the need for complex computer algebra caused by the spin terms in the D-Hamiltonian. Apart from this, a post-DHF treatment for electron correlation may suffer from the *Brown-Ravenhall disease*,[46] which originates from the fact that for any perturbational solution one must include the negative energy eigenstates. Hence, all two-electron states with one electron at $E_1 < -2mc^2$ and the other having a positive energy E_2 are degenerate (because of the large gap of $2mc^2$) thus causing a breakdown of perturbation theory. Sucher[47] has described this problem as *continuum dissolution* because in the two-electron system a transition becomes possible which ejects one electron into the positive continuum. The continuum dissolution applies to both the DC and the DCB Hamiltonian.

When solving chemical problems, only the positive (electronic) eigenstates and the positive continuum of the DC-Hamiltonian are of relevance, and therefore modern relativistic quantum chemistry is based on *no-pair* Hamiltonians, i.e., a relativistic description that excludes electron–positron pair-creations that become possible when the negative eigenstates are included.[1] This is in line with the necessity of simplifying the Dirac 4-component

calculations so that larger molecules can be investigated. Already early attempts focused on eliminating the small component Ψ^S, caused by the positronic states, from the wave function. This can be done in an exact way for a free electron utilizing the Foldy-Wouthuysen transformation, which is based on a series of unitary transformations of the D-Hamiltonian.[48] For bound electrons in atoms or molecules, however, the Foldy-Wouthuysen transformation can only be approximated or replaced by other techniques. In the 1980s and 1990s, perturbation theory was preferentially employed to obtain quasi-relativistic approximations with two- or just one-component wave functions, where the latter corresponded to a *spin-free* description.[1]

The basic idea of the quasi-relativistic methods is to approximate the Foldy-Wouthuysen transformation by expanding it in powers of V (nucleus–electron attraction potential) or in powers of

$$\frac{\epsilon}{2mc^2 - V} \tag{5}$$

where ϵ is the energy of the one-particle Dirac equation. The former approach was pursued by Douglas and Kroll in 1974[49] and, later in the 1980s and 1990s, extended by Hess so that low orders n of the so-called *Douglas-Kroll-Hess* (DKH) method could be developed.[50–53] As in the case of the Foldy-Wouthuysen transformation, the DKH transformation cannot be given in closed form and accordingly requires a number of transformations U_0, U_1, $\cdots$ thus leading to a decoupling of the electronic from the positronic states and with each transformation to increasing accuracy. When however higher orders of the DKH method[54,55] are worked out, it becomes obvious that the DKHn theory (DKH of order n) suffers from slow convergence and mathematical complexity.

These convergence problems are not experienced when using a perturbation expansion in terms of expression (5), which is the basis of the so-called *Regular Approximation* (*RA*) to the relativistic Hamiltonian and which provides rapid convergence to the Dirac one-electron energy.[56] However, the RA suffers from technical problems due to the fact that the potential energy V appears in the denominator of (5). Originally, the methods based on the RA were formulated by Baerends and co-workers[57–59] on numeric quadratures in connection with density functional theory (DFT) in the form of the zero-order regular approximation (ZORA) and the first-order regular approximation (FORA) method. An improvement of ZORA was obtained by developing an approach for which the relativistic normalization of the wave function is carried out at infinite order and which therefore was dubbed (rather misleading) IORA (Infinite Order Regular Approximation).[60] Hence, ZORA and IORA are based on the same Hamiltonian but use different wave function metrics. Originally, ZORA and IORA suffered from three serious shortcomings: (1) The relativistic one-electron integrals of ZORA (IORA) could only be obtained using numeric quadratures, which hampered an extension of these methods beyond the DFT realm; (2) ZORA (IORA) results suffered from an electrostatic gage-dependence, i.e., they depended on where the zero of the potential is chosen; and (3) it was not clear how in a simple and economical way the RA methods could be improved so that a Dirac-exact relativistic result would become available.

Some of the shortcomings of ZORA and IORA were overcome by Filatov and Cremer, who developed matrix representations of the ZORA and IORA Hamiltonians,[61–64] derived their relationship to an exact quasi-relativistic Hamiltonian,[65] and solved the gage-dependence problem of ZORA and IORA.[66] Although only low orders of the RA were implemented, the development of the latter had an important impact on the derivation of a Dirac-exact relativistic method applicable to large molecules containing relativistic atoms.[65,67] Other approximate quasi-relativistic methods were developed, which are described in the relevant literature.[1–3,9,10,12–14]

DIRAC-EXACT RELATIVISTIC METHODS

By definition a Dirac-exact relativistic method is a quasi-relativistic 2- or 1-component method which exactly reproduces the one-electron energies of the original 4-component Dirac method,[37,38] where the starting wave function can be of the HF or KS type. In the following, we will speak of Dirac-exact methods without emphasizing always their quasi-relativistic nature. It is desirable to develop a Dirac-exact relativistic method in such a way that it can be smoothly integrated in the toolbox of nonrelativistic theory. This concerns the use of (1) correlation methods for determining dynamic and nondynamic electron correlation; (2) methods and techniques of calculating response properties; and (3) methods to describe excited states.

As pointed out in the previous section, one of the major objectives pursued during the last 15 years in relativistic quantum chemistry was the derivation of Dirac-exact relativistic methods which do not require the solution of Dirac's 4-component equation.[37,38]

This objective was first achieved by Dyall,[68] who developed the NESC method as the first Dirac-exact 2-component relativistic approach. With NESC, Dyall accomplished two objectives. First, he projected the exact relativistic one-electron D-Hamiltonian[37] onto the positive-energy (electronic) states to get a Dirac-exact 2-component representation. Second, he separated the spin part of the D-Hamiltonian to obtain a 1-component, spin-free representation.

NESC requires just one transformation matrix **U** to eliminate the small component and accordingly only one Fock matrix **F**, which however was originally calculated in an iterative manner where for each iteration step a new relativistic metric $\widetilde{\mathbf{S}}$ had to be determined (because of its dependence on **U**, see below). In his 1997 publication, Dyall calculated only the one-electron Ne^{9+} ion, however, the corresponding results revealed already the advantages of the NESC method compared to perturbative approaches such as DKHn or ZORA (IORA).[68]

Dyall based his development on two-important innovations: (1) He introduced a matrix representation of the Dirac equation. This was a novel approach because most previous development work had focused on an operator presentation of the effects of relativity. By switching to a matrix presentation, he implicitly introduced a description of the relativistic problem by a finite basis set with all the problems accompanying such a step (basis set truncation error, singularity problem at the point-nucleus, etc.). However, writing the Dirac equation in matrix form proved to be essential for an elimination of the small component. (2) He rewrote the Dirac equation and obtained what is known today as the *modified Dirac equation*.[1,68] Steps (1) and (2) were important for deriving the NESC equations.

Dyall's work triggered in the following years a number of developments, which led to a number of Dirac-exact relativistic methods that could routinely be applied for the relativistic quantum chemical description of large molecules and their properties:

- In the years 1999–2002, Dyall simplified the solution of the NESC equations by fixing the ratio of the large to the small component (and thereby matrix **U**) in atomic calculations, thus yielding approximate NESC energies but effectively reducing the calculational load of the NESC description for molecules.[69,70]
- From 2002 on, Wolf et al. mastered the problems of high-order DKHn calculations by developing an infinite order DKHn theory, which reproduced exact 4-component Dirac energies.[71–75] The infinite order theory offered in this regard an important improvement of DKH and represented a Dirac-exact method.
- In the years 2005–2007, Kutzelnigg and Liu classified quasi-relativistic methods as being operator-based or matrix-based and pointed out in this connection that the latter lead in a much easier way to Dirac-exact relativistic descriptions.[45,76,77] These authors established the basic requirements for exact 2-component relativistic methods, for which the term X2C was coined.[78]
- In the same time period, the Infinite-Order Two-Component (IOTC) method, which was originally developed by Barysz et al.[79] using operator algebra and which had already been extensively used,[80–83] was converted into matrix algebra by Iliaš and co-workers.[84] Iliaš and Saue[85] and Barysz et al.[86] demonstrated that IOTC also provides Dirac-exact energies.
- In 2006, Filatov[87] emphasized that Dyall's 2-component NESC method[68] fulfills the criteria of an exact X2C method and therefore its practical realization, accomplished in the year 2007 by introducing a new iterative algorithm for solving the NESC equations,[88] was considered as making X2C calculations generally available. Kutzelnigg and Liu[89] identified NESC also as an X2C method, but criticized the unnormalized version of NESC (UESC), which had also been discussed in Dyall's original NESC paper.[68] This was relevant in connection with ZORA, which can be considered as an UESC-ZORA method, whereas IORA corresponds to a NESC-ZORA method as had been pointed out by Filatov and Cremer.[67]
- In 2011, the computational difficulties still accompanying the solution of the NESC equations were finally solved by Zou, Filatov and Cremer (ZFC),[44] which made obsolete the atom-centered approximation to NESC developed by Dyall and Enevoldsen,[69] the iterative approach by Filatov and Dyall,[88] and the early low-order NESC approximations of Filatov and Cremer.[90,91] Part of the success of ZFC[44] was based on the use of IORA as a convenient starting point for an iterative solution of the NESC equations.[67]
- In the following years, ZFC converted NESC to a generally applicable method[44] that can be used for the routine calculation of first-order response properties (molecular geometries,[92–94] electric dipole moment,[95] electric field gradients,[96] hyperfine structure constants,[97] contact densities

and Mössbauer shifts,[98] etc.) and second-order response properties (vibrational frequencies,[95,99] electric polarizabilities,[95] infrared intensities,[95] etc.)

- Parallel and independently, Gauss and Cheng developed methods to calculate molecular geometries, vibrational frequencies, and magnetic properties at the level of Dirac-exact methods.[100–102]
- In 2013, Filatov, Zou, and Cremer (FZC) extended the spin-free 1-component NESC method to a 2-component method to calculate SOC effects.[103]

In the following, we will focus on the description of these last steps and in this way present an updated account on the applicability of Dirac-exact methods such as NESC. In this connection, we will consider first the spin-free approach, which includes only scalar relativistic effects and in a later section also the 2-component NESC method. In view of the accomplishments of Dyall in connection with Dirac-exact relativistic methods, we stick to the acronym NESC rather than using the acronym X2C (for an exact 2-component method), which is preferred by some authors, however, sometimes indiscriminately for 1- and 2-component methods.

THE NESC EIGENVALUE PROBLEM AND ITS SOLUTION

Dyall's derivation of a spin-free NESC equation[68] is based on the no-pair approximation (which guarantees that negative eigenstates do not intrude the space of the positive eigenstates[1,3]) and the definition of a pseudo-large component of the wave function, Φ^{L}, for the purpose of eliminating the small component:

$$2mc\Psi^{\mathrm{S}} = (\boldsymbol{\sigma}\cdot\mathbf{p})\,\Phi^{\mathrm{L}} \tag{6}$$

Equation 6 is not unique, but has the advantage of making the relativistic metric $\widetilde{\mathbf{S}}$ spin-free.[1] This simplifies the partitioning of the D-Hamiltonian into spin-free and a spin-dependent part (the latter describing the SOC effects), which was first discussed by Kutzelnigg[104] and later by Dyall.[105]

The modified Dirac equation in matrix notation takes the form

$$\begin{pmatrix} \mathbf{V} & \mathbf{T} \\ \mathbf{T} & \mathbf{W}-\mathbf{T} \end{pmatrix} \begin{pmatrix} \mathbf{A}_{\mathrm{p}} & \mathbf{A} \\ \mathbf{B}_{\mathrm{p}} & \mathbf{B} \end{pmatrix} = \begin{pmatrix} \mathbf{S} & \mathbf{0} \\ \mathbf{0} & (2mc^2)^{-1}\mathbf{T} \end{pmatrix} \begin{pmatrix} \mathbf{A}_{\mathrm{p}} & \mathbf{A} \\ \mathbf{B}_{\mathrm{p}} & \mathbf{B} \end{pmatrix} \begin{pmatrix} \mathbf{E}_{\mathrm{p}} & \mathbf{0} \\ \mathbf{0} & \mathbf{E} \end{pmatrix} \tag{7}$$

Here, matrices $\mathbf{A}$ and $\mathbf{B}$ collect the eigenvectors of the large and pseudo-large component (with subscript p: positronic; without: electronic). They are related via the matrix $\mathbf{U}$ according to Eq. (8.[68])

$$\mathbf{B} = \mathbf{U}\mathbf{A} \tag{8}$$

In Eq. (7), E_{p} and E denote the positronic (negative) and electronic (positive) eigenvalues, respectively. Matrices $\mathbf{T}$, $\mathbf{V}$, and $\mathbf{S}$ correspond to the nonrelativistic kinetic energy, potential energy (nucleus–electron attraction), and overlap matrix, respectively. $\mathbf{W}$ is the negative definite matrix of the operator $(1/4m^2c^2)\boldsymbol{\sigma}\cdot\mathbf{p}V(\mathbf{r})\boldsymbol{\sigma}\cdot\mathbf{p}$, which simplifies in the scalar relativistic approximation to $(1/4m^2c^2)\nabla V(\mathbf{r})\cdot\nabla$ and which can be easily derived from the derivatives of the potential energy integrals.

The elimination of the small component via the pseudo-large component is the key for deriving the NESC equation, which can be written in the simple form[68]

$$\widetilde{\mathbf{L}}\mathbf{A} = \widetilde{\mathbf{S}}\mathbf{A}\boldsymbol{\epsilon} \tag{9}$$

Here, $\widetilde{\mathbf{L}}$ is the matrix of the NESC Hamiltonian, $\boldsymbol{\epsilon}$ is the diagonal matrix of the NESC eigenvalues, $\mathbf{A}$ has been defined in connection with Eq. (7), and the relativistic metric $\widetilde{\mathbf{S}}$ is given by

$$\widetilde{\mathbf{S}} = \mathbf{S} + \frac{1}{2mc^2}\mathbf{U}^{\dagger}\mathbf{T}\mathbf{U} \tag{10}$$

The eigenvectors of the large component are normalized on the relativistic metric according to

$$\mathbf{A}^{\dagger}\widetilde{\mathbf{S}}\mathbf{A} = \mathbf{I} \tag{11}$$

The NESC Hamiltonian matrix is given by

$$\widetilde{\mathbf{L}} = \mathbf{T}\mathbf{U} + \mathbf{U}^{\dagger}\mathbf{T} - \mathbf{U}^{\dagger}(\mathbf{T}-\mathbf{W})\,\mathbf{U} + \mathbf{V} \tag{12}$$

which shows that both $\widetilde{\mathbf{L}}$ and $\widetilde{\mathbf{S}}$ depend on matrix $\mathbf{U}$, i.e., the matrix of the small component elimination operator. The calculation of $\mathbf{U}$ is the key problem of solving the NESC equation. Work by Dyall,[68] Filatov and Cremer,[67] Filatov and Dyall,[88] and ZFC[44] has stepwise improved the solution of this problem where in all cases the IORA solution[60,67] is taken as the starting point for the calculation of $\mathbf{U}$.

$$\widetilde{\mathbf{L}}^{\mathrm{IORA}}\mathbf{A}^{\mathrm{IORA}} = \widetilde{\mathbf{S}}^{\mathrm{IORA}}\mathbf{A}^{\mathrm{IORA}}\boldsymbol{\epsilon}^{\mathrm{IORA}} \tag{13}$$

Here, the matrix of the IORA Hamiltonian $\widetilde{\mathbf{L}}^{\mathrm{IORA}}$ and the IORA metric $\widetilde{\mathbf{S}}^{\mathrm{IORA}}$ are obtained with

the help of Eq. (14,[67])

$$\mathbf{U}^{\mathrm{IORA}} = (\mathbf{T} - \mathbf{W})^{-1}\,\mathbf{T} \tag{14}$$

and by inserting $\mathbf{U}^{\mathrm{IORA}}$ into the IORA-equivalent of Eqs (12) and (10). Because $\mathbf{W}$ is a negative definite matrix (see above), Eq. (14) does not diverge. It has been shown by ZFC that matrix $\mathbf{U}$ can be expressed via $\mathbf{U}^{\mathrm{IORA}}$ as[44]

$$\mathbf{U} = \mathbf{U}^{\mathrm{IORA}}\left[\mathbf{I} - \frac{1}{2mc^2}\mathbf{U}\mathbf{S}^{-1}\,(\mathbf{T}\mathbf{U} + \mathbf{V})\right] \tag{15}$$

This is the key equation for determining $\mathbf{U}$ by either a one-step or an iterative method.

Solution of the NESC Equation Via the Riccati Equation: The One-Step Method

The one-step method was first suggested by Dyall[68] and later used by other authors.[45,81,85] The method is based on the fact that Eq. (15) can be rewritten in the form

$$\mathbf{U}\left(\frac{1}{2mc^2}\mathbf{S}^{-1}\mathbf{T}\right)\mathbf{U} + \left(\mathbf{U}^{\mathrm{IORA}}\right)^{-1}\mathbf{U} + \mathbf{U}\left(\frac{1}{2mc^2}\mathbf{S}^{-1}\mathbf{V}\right) - \mathbf{I} = 0 \tag{16}$$

which corresponds to a nonsymmetric algebraic Riccati equation:[106]

$$\mathbf{U}\alpha\mathbf{U} + \beta\mathbf{U} + \mathbf{U}\gamma + \delta = 0 \tag{17}$$

where $\boldsymbol{\alpha}$, $\boldsymbol{\beta}$, $\boldsymbol{\gamma}$, and $\boldsymbol{\delta}$ are known matrices. Using standard procedures, the unknown matrix $\mathbf{U}$ can be determined.[106] This implies the transformation of the M-dimensional quadratic equation into the 2 M-dimensional matrices of the Dirac equation (7). Solving Eq. (7) by diagonalization provides all needed eigenvalues and eigenvectors. Then, the matrix $\mathbf{U}$ is directly determined with the help of Eq. (8). Once $\mathbf{U}$ is known, the NESC matrices $\widetilde{\mathbf{S}}$ and $\widetilde{\mathbf{L}}$ can be obtained from Eqs. (10) and (12).

Iterative Solution of the NESC Equation: The TU Algorithm

Since the calculation of matrix $\widetilde{\mathbf{L}}$ depends on $\mathbf{U}$ and that of $\mathbf{U}$ on $\widetilde{\mathbf{L}}$, an iterative determination of the former becomes obvious. Starting from Eq. (15), ZFC[44] expanded $\widetilde{\mathbf{L}}$ in terms of $\mathbf{Z} = \mathbf{T}\mathbf{U}$ thus yielding

$$\widetilde{\mathbf{L}} = \mathbf{Z} + \mathbf{Z}^{\dagger} - \mathbf{Z}^{\dagger}\left(\mathbf{T}^{-1} - \mathbf{T}^{-1}\mathbf{W}\mathbf{T}^{-1}\right)\mathbf{Z} + \mathbf{V} \tag{18}$$

$$\mathbf{Z} = \mathbf{S}\widetilde{\mathbf{S}}^{-1}\widetilde{\mathbf{L}} - \mathbf{V} \tag{19}$$

$$\widetilde{\mathbf{S}} = \mathbf{S} + \frac{1}{2mc^2}\mathbf{Z}^{\dagger}\mathbf{T}^{-1}\mathbf{Z}, \tag{20}$$

By applying a fixed-point iteration with a damping parameter α according to[44]

$$\mathbf{Z}^{(n)} = f\left(\mathbf{Z}^{(n-1)}\right) - \alpha\left(f\left(\mathbf{Z}^{(n-1)}\right) - \mathbf{Z}^{(n-1)}\right) \tag{21}$$

first the product $\mathbf{TU}$ and then, with the help of the known matrix $\mathbf{T}$, $\mathbf{U}$ was determined. Convergence was monitored by comparing the absolute differences in the diagonal elements of the NESC Hamiltonian matrix (18) from successive iterations.

Comparison of the one-step and iterative method revealed that the former is of advantage in energy calculations with less than 1000 basis functions, whereas the latter reduces computational costs for large basis set calculations, geometry optimizations, and reaction path calculations.[44]

Renormalization of the Wave Function: The Picture-Change

The NESC equation provides the Dirac-exact solution of the one-electron problem. In the context of the DC-Hamiltonian for many-electron systems, the NESC one-electron Hamiltonian can be combined with the nonrelativistic two-electron part, which leads to the so-called *one-electron approximation*.[70,107] This implies, however, that the one-electron NESC Hamiltonian is renormalized on the nonrelativistic metric with the help of a renormalization matrix $\mathbf{G}$:[70,107]

$$\mathbf{H}_{1-e} = \mathbf{G}^{\dagger}\widetilde{\mathbf{L}}\mathbf{G} \tag{22}$$

Equation (22) guarantees that $\mathbf{H}_{1-e}$ (set up in the relativistic picture) can be applied in connection with the HF or KS equations (defined in a nonrelativistic picture). This *picture-change* caused by switching from the relativistic Dirac–Pauli representation to the nonrelativistic Newton–Wigner representation is correctly handled by a renormalization matrix $\mathbf{G}$ derived by Liu and Peng,[78]

$$\mathbf{G} = \mathbf{S}^{-1/2}\left(\mathbf{S}^{1/2}\widetilde{\mathbf{S}}^{-1}\mathbf{S}^{1/2}\right)^{1/2}\mathbf{S}^{1/2} \tag{23}$$

Picture change effects may not be large for relative energies (dominated by the properties of the valence electrons), but become large when properties depending on a close distance from the nucleus have

to be determined. The total electronic energy at the HF level is given by Eq. (24),

$$E = \mathrm{tr}\,[\mathbf{P}\mathbf{H}_{1-e}] + \frac{1}{2}\mathrm{tr}\,[\mathbf{P}\,(\mathbf{J}-\mathbf{K})] \tag{24}$$

where **J** and **K** are the Coulomb and the exchange parts of the Fock matrix and **P** is the density matrix calculated as $\mathbf{P} = \mathbf{C}\mathbf{n}\mathbf{C}^{\dagger}$ with **C** collecting the eigenvectors of the Fock matrix and **n** being the diagonal matrix of the orbital occupation numbers.

First-Diagonalize-Then-Contract Strategy

When using a basis with a sufficiently large number of primitive Gaussian functions M_p, the exact solutions of the Dirac equation for one electron can be reproduced with sufficient accuracy.[44,68,107] For many-electron systems, use of a large number of primitive basis functions leads to an M_p^4 increase in the number of two-electron integrals and high computational cost. Cost reduction is achieved in these cases by using contracted basis sets (M_c basis functions with $M_\mathrm{c} << M_\mathrm{p}$). For the purpose of solving this dichotomy, the following procedure was used by ZFC:[44] The NESC one-electron equations were solved in the basis set of M_p primitive basis functions and the renormalized one-electron Hamiltonian (22) was converted to a contracted basis set with M_c functions. This *First-Diagonalize-then-Contract* strategy has some advantages:[44] (1) The completeness requirement is better fulfilled; (2) Computational costs are not significantly increased to those of a nonrelativistic HF or KS calculation; (3) variational collapse that can emerge when using strongly contracted basis functions[108] no longer occurs; and (4) inverse variational collapse problems, which may occur when using uncontracted basis sets with very steep basis functions, can easily be handled by using a finite nucleus model.

The Finite Nucleus Model

In the case of a nonrelativistic treatment, the orbitals have a cusp at the position of a point charge nucleus, which for a relativistic treatment converts into a singularity. The latter is difficult to describe with a basis set comprising Gaussian-type functions. By introducing a nuclear model with a finite size of the nucleus, the singularity is removed, thus leading to a better description of the region close to the nucleus. Although the finite size nucleus has a charge distribution closer to a Fermi-Dirac distribution (a liquid drop with a diffuse surface),[109] one assumes, because of practical reasons, a spherically symmetric charge distribution, which can be represented by a Gaussian-type function[110,111] according to

$$\rho_A(r) = Z_A\left(\frac{1}{\pi\zeta^2}\right)^{3/2} \mathrm{e}^{-r^2/\zeta^2} \tag{25}$$

Using the function of Eq. (25), the electron-nuclear interaction potential $v(\mathbf{r}-\mathbf{R}_K)$ ($\mathbf{R}_K$: position vector of nucleus K) is given by Eq. (26)

$$v(\mathbf{r}-\mathbf{R}_K) = -\frac{1}{|\mathbf{r}-\mathbf{R}_K|}\mathrm{erf}\left(\frac{|\mathbf{r}-\mathbf{R}_K|}{\zeta_K}\right) \tag{26}$$

where erf is the error function and ζ_K is introduced as a parameter, which can be derived from the measured root mean square (rms) charge radius $\langle R_K^2\rangle^{1/2}$ of nucleus K using Eq. (27):

$$\zeta_K = \sqrt{\frac{2}{3}}\left\langle R_K^2\right\rangle^{1/2} \tag{27}$$

The Coulomb potential of a point-charge model of the nucleus used in nonrelativistic quantum chemistry is recovered by setting $\zeta_K = 0$. New molecular integrals of the type $\langle\chi_\mu|v(\mathbf{r}-\mathbf{R}_K)|\chi_\nu\rangle$ have to be calculated, which however does not pose any problem.[44]

Of course, the assumption of a Gaussian charge distribution and the determination of the exponent of the corresponding Gaussian function via the measured root-mean square radius of the nucleus[110,111] can only be considered as an approximation since the exact charge distribution in the nucleus is not known. For example, the Zemach radius of a nucleus,[112] i.e., the magnetic nuclear radius, is more appropriate when calculating magnetic properties. In any case, use of a finite nuclear model leads to relatively large changes in the total energy, whereas properties depending preferentially on the valence electrons (e.g., bond lengths, vibrational frequencies) do not change significantly.[92,99]

Comparison of NESC Energies with 4-Component Dirac Results

In Table 1, NESC Hartree-Fock (HF) energies of hydrogen-like ions with atomic numbers $Z = 20$, 40, ..., 120 are compared with those of 4-component DHF and quasi-relativistic calculations.[44] NESC reproduces the 4-component DHF atomic energies in all cases, which confirms that NESC is a Dirac-exact relativistic method.

Perturbational approaches such as DKHn or RA-based methods, which do not provide an upper

TABLE 1 | Ground State Energies (in Hartree) of Hydrogen-Like Ions Calculated with Different 4-Component (4c) and 1-Component Relativistic Methods

Method	$Z=20$	40	60	80	100	120
Point charge nuclear model with 50 s-functions[1]						
4c-DHF(UKB)	−201.076522	−817.807491	−1895.68234	−3532.19213	−5939.19514	−9710.71531
NESC	−201.076522	−817.807491	−1895.68234	−3532.19213	−5939.19514	−9710.71531
Approximate methods						
ZORA[67]	−202.158829	−836.011368	−1996.45087	−3898.86916	−7054.8079	−13096.9617
IORA[67]	−201.082194	−818.171957	−1899.90000	−3536.90102	−6042.5850	−10089.4142
NESC-SORA[67]	−201.076522	−817.807633	−1895.68972	−3532.31224	−5940.2749	−9718.0099
DKH2[74]	−201.072540	−817.615780	−1893.89769	−3523.32490	−5906.1919	−9594.1000
DKH3[74]	−201.076662	−817.820117	−1895.84407	−3533.11958	−5942.3695	−9712.9340
DKH14[74]	−201.076523	−817.807497	−1895.68235	−3532.19184	−5939.1821	−9710.2510
Finite nuclear model with 50 s-functions[2]						
4c-DHF(UKB)	−201.076001	−817.788172	−1895.45071	−3530.19419	−5922.78995	−9545.87512
NESC	−201.076001	−817.788172	−1895.45071	−3530.19419	−5922.78995	−9545.87512

[1]UKB: unrestricted kinetic balance. See Ref 44.
[2]Ref 44. Mass number of isotope was taken from Ref 111. For $Z=120$, mass number $=2.556\times Z=306.72$.

bound to the correct DHF energy, approach the exact results in an oscillatory manner, overestimating or underestimating exact atomic energies. This is also reflected by the data in Table 1. For $Z\leq 60$, DKHn atomic energies with $n=14$ are close to the exact values, whereas for $Z>60$, one has to apply DKHn with $n>20$ to obtain accurate values. Infinite order DKH theory correctly reproduces DHF (and NESC) energies. However, it becomes also obvious that convergence of the DKHn energies to the correct result is rather slow.[44]

Methods based on the RA converge much faster, but largely overshoot exact results at the ZORA and IORA levels of theory. The development of a matrix formulation for the methods based on the RA by Filatov and Cremer made it possible to consider second- and third-order IORA methods[65] and to connect the RA directly to NESC, for example, via the NESC-SORA (second-order regular approximation) method. NESC-SORA provides exact results for small Z, whereas for larger Z its energies again overshoot exact DHF energies.

As mentioned before, the relativistic calculations benefit from a finite nucleus model rather than a 0-radius (point charge) model.[1,44,111] For example, the singularity of the Dirac equation at the position of the nucleus caused by the point charge model is avoided. The increase in energy as described by the 4-component DHF method is correctly reproduced by the NESC method (Table 1).

FIRST-ORDER RESPONSE PROPERTIES

The usefulness of a new quantum chemical method is measured by its accuracy and general applicability. General applicability implies the possibility of routinely calculating molecular properties such as geometries, vibrational frequencies, electric or magnetic quantities, excitation energies, etc. A large number of molecular properties needed by chemists to analyze and characterize structure, stability, and reactivity of a chemical compound are response properties, which can be effectively calculated with the help of analytical energy derivatives.[113] Accordingly, the usefulness of a quantum mechanical method increases substantially when its applicability range is extended by the introduction of analytical energy derivatives.

Derivation of the NESC Gradient

The first derivative of the total energy, Eq. (24), with respect to a parameter λ, which can correspond to a nuclear coordinate or a component of the electric field or another external perurbation, is given by Eq. (28)[114]

$$\frac{\partial E}{\partial\lambda}=\mathrm{tr}\left[\mathbf{\Omega}\frac{\partial \mathbf{S}}{\partial\lambda}\right]+\mathrm{tr}\left[\mathbf{P}\frac{\partial \mathbf{H}_{1-e}}{\partial\lambda}\right]+\frac{1}{2}\mathrm{tr}\left[\mathbf{P}\frac{\partial'}{\partial\lambda}(\mathbf{J}-\mathbf{K})\right] \tag{28}$$

Here, matrix Ω is defined by $\Omega = -\mathbf{C}\boldsymbol{\epsilon}\mathbf{n}\mathbf{C}^{\dagger}$, and the prime at $\partial'/\partial\lambda$ implies that only the two-electron integrals rather than the density matrix need to be differentiated. The first and the last term on the right hand side (r.h.s.) are calculated utilizing the nonrelativistic methodology. Only the second term has to be determined in a NESC gradient calculation. This was first done by ZFC[92] and somewhat later by Cheng and Gauss.[100]

The second term in Eq. (28) has the form[92]

$$\mathrm{tr}\left[\mathbf{P}\frac{\partial \mathbf{H}_{1-e}}{\partial\lambda}\right] = \mathrm{tr}\left[\widetilde{\mathbf{P}}\frac{\partial \widetilde{\mathbf{L}}}{\partial\lambda}\right] + \mathrm{tr}\left[\mathbf{D}\frac{\partial \mathbf{G}^{\dagger}}{\partial\lambda}\right] + \mathrm{tr}\left[\mathbf{D}^{\dagger}\frac{\partial \mathbf{G}}{\partial\lambda}\right] \tag{29}$$

where the new matrices $\widetilde{\mathbf{P}} = \mathbf{G}\mathbf{P}\mathbf{G}^{\dagger}$ and $\mathbf{D} = \widetilde{\mathbf{L}}\mathbf{G}\mathbf{P}$ are introduced. Hence, the derivative of the NESC Hamiltonian matrix $\widetilde{\mathbf{L}}$ and the renormalization matrix $\mathbf{G}$ are required for calculating the NESC energy gradient. For the first term in Eq. (29), one obtains:

$$\begin{aligned}\mathrm{tr}\left[\widetilde{\mathbf{P}}\frac{\partial \widetilde{\mathbf{L}}}{\partial\lambda}\right] &= \mathrm{tr}\left[\left(\mathbf{U}\widetilde{\mathbf{P}} + \widetilde{\mathbf{P}}\mathbf{U}^{\dagger} - \mathbf{U}\widetilde{\mathbf{P}}\mathbf{U}^{\dagger}\right)\frac{\partial \mathbf{T}}{\partial\lambda}\right] \\ &+ \mathrm{tr}\left[\left(\mathbf{U}\widetilde{\mathbf{P}}\mathbf{U}^{\dagger}\right)\frac{\partial \mathbf{W}}{\partial\lambda}\right] + \mathrm{tr}\left[\widetilde{\mathbf{P}}\frac{\partial \mathbf{V}}{\partial\lambda}\right] \\ &+ \mathrm{tr}\left[\left(\mathbf{P}^{L}\right)^{\dagger}\frac{\partial \mathbf{U}^{\dagger}}{\partial\lambda} + \mathbf{P}^{L}\frac{\partial \mathbf{U}}{\partial\lambda}\right]\end{aligned} \tag{30}$$

where $\mathbf{P}^{L} = \widetilde{\mathbf{P}}\left[\mathbf{T} - \mathbf{U}^{\dagger}(\mathbf{T} - \mathbf{W})\right]$. The calculation of the first three terms on the r.h.s. of Eq. (30) is straightforward because the one-electron integral derivatives are directly available from nonrelativistic quantum chemical methods. The major difficulty results from term four, which contains the derivatives $\partial\mathbf{U}/\partial\lambda$. The $\mathbf{U}$ derivatives also appear in $\partial\mathbf{G}/\partial\lambda$ because $\mathbf{G}$ depends on $\widetilde{\mathbf{S}}$ and $\widetilde{\mathbf{S}}$ on $\mathbf{U}$ (see Eqs 23 and 10).

By collecting all contributions $\partial\mathbf{U}/\partial\lambda$ from $\widetilde{\mathbf{L}}$ and $\mathbf{G}$, one obtains a relatively simple equation:[92]

$$\begin{aligned}&\mathrm{tr}\left(\mathbf{P}^{L}\frac{\partial \mathbf{U}}{\partial\lambda} + \left(\mathbf{P}^{L}\right)^{\dagger}\frac{\partial \mathbf{U}^{\dagger}}{\partial\lambda}\right) + \mathrm{tr}\left(\mathbf{P}^{G}\frac{\partial \mathbf{U}^{\dagger}}{\partial\lambda}\mathbf{U} + \mathbf{P}^{G}\mathbf{U}^{\dagger}\frac{\partial \mathbf{U}}{\partial\lambda}\right) \\ &= \mathrm{tr}\left(\mathbf{P}_0\frac{\partial \mathbf{U}}{\partial\lambda} + \mathbf{P}_0^{\dagger}\frac{\partial \mathbf{U}^{\dagger}}{\partial\lambda}\right)\end{aligned} \tag{31}$$

where matrices $\mathbf{P}^{G}$ and $\mathbf{P}^{L}$ have been defined in the original literature.[92] By writing Eq. (15) in the form

$$\mathbf{U} = \mathbf{U}^{\mathrm{IORA}} - \frac{1}{2mc^2}\mathbf{U}^{\mathrm{IORA}}\mathbf{U}\mathbf{S}^{-1}(\mathbf{T}\mathbf{U} + \mathbf{V}) \tag{32}$$

the partial derivative of $\mathbf{U}$ with regard to λ is obtained as

$$\begin{aligned}\frac{\partial \mathbf{U}}{\partial\lambda} &= \frac{\partial \mathbf{U}^{\mathrm{IORA}}}{\partial\lambda}\left(\mathbf{U}^{\mathrm{IORA}}\right)^{-1}\mathbf{U} - \frac{1}{2mc^2}\mathbf{U}^{\mathrm{IORA}} \\ &\times\left[\frac{\partial \mathbf{U}}{\partial\lambda}\mathbf{S}^{-1}(\mathbf{T}\mathbf{U} + \mathbf{V}) + \mathbf{U}\frac{\partial \mathbf{S}^{-1}}{\partial\lambda}(\mathbf{T}\mathbf{U} + \mathbf{V})\right. \\ &\left.+\mathbf{U}\mathbf{S}^{-1}\left(\frac{\partial \mathbf{T}}{\partial\lambda}\mathbf{U} + \mathbf{T}\frac{\partial \mathbf{U}}{\partial\lambda} + \frac{\partial \mathbf{V}}{\partial\lambda}\right)\right]\end{aligned} \tag{33}$$

This equation can be brought in the form of the Sylvester equation.[92,99]

Solution of the Gradient Problem Via the Sylvester Equation: The One-Step Method

The Sylvester equation has the form[99]

$$\mathbf{A}\mathbf{X} + \mathbf{X}\mathbf{B} = \mathbf{C} \tag{34}$$

If matrix $\mathbf{X}$ contains the derivatives $\partial\mathbf{U}/\partial\lambda$, then[99]

$$\mathbf{A} = \mathbf{I} - \mathbf{T}^{-1}\mathbf{W} + \frac{1}{2mc^2}\mathbf{U}\mathbf{S}^{-1}\mathbf{T} \tag{35}$$

$$\mathbf{B} = \frac{1}{2mc^2}\mathbf{S}^{-1}(\mathbf{T}\mathbf{U} + \mathbf{V}) \tag{36}$$

$$\begin{aligned}\mathbf{C} &= -\mathbf{T}^{-1}\frac{\partial \mathbf{T}}{\partial\lambda}\mathbf{T}^{-1}\mathbf{W}\mathbf{U} + \mathbf{T}^{-1}\frac{\partial \mathbf{W}}{\partial\lambda}\mathbf{U} \\ &+\frac{1}{2mc^2}\mathbf{U}\mathbf{S}^{-1}\left[\frac{\partial \mathbf{S}}{\partial\lambda}\mathbf{S}^{-1}(\mathbf{T}\mathbf{U} + \mathbf{V}) - \frac{\partial \mathbf{T}}{\partial\lambda}\mathbf{U} - \frac{\partial \mathbf{V}}{\partial\lambda}\right]\end{aligned} \tag{37}$$

Depending on what response properties are required, the Sylvester equation can be solved in a one-step procedure or by an iterative procedure according to

$$\mathbf{X}_{n+1} = \mathbf{A}^{-1}\mathbf{C} - \mathbf{A}^{-1}\mathbf{X}_n\mathbf{B} \tag{38}$$

The latter is the method of choice, e.g., for geometry optimizations. However, for higher accuracy, especially in the case of very steep basis functions (exponents $|\zeta| > 10^{12}$) and a point-nucleus model the eigenvalue decomposition method is preferable, which is more costly, but numerically more stable. The latter method has been used by several authors[63,101,115] and was also applied by ZFC.[99]

For high accuracy calculations which are required, e.g., when determining contact densities (see below), a more efficient method is based on

response theory. For this purpose, ZFC rewrote the Dirac equation in the following form:[99]

$$\tilde{\mathbf{D}}\mathbf{\Phi} = \tilde{\mathcal{S}}\mathbf{\Phi}\epsilon \tag{39}$$

with

$$\tilde{\mathbf{D}} = \begin{pmatrix} \mathbf{V} & \mathbf{T} \\ \mathbf{T} & \mathbf{W} - \mathbf{T} \end{pmatrix} \tag{40}$$

$$\tilde{\mathcal{S}} = \begin{pmatrix} \mathbf{S} & \mathbf{0} \\ \mathbf{0} & (2mc^2)^{-1}\,\mathbf{T} \end{pmatrix} \tag{41}$$

$$\mathbf{\Phi} = \begin{pmatrix} \mathbf{A}_\mathrm{p} & \mathbf{A} \\ \mathbf{B}_\mathrm{p} & \mathbf{B} \end{pmatrix} \tag{42}$$

$$\epsilon = \begin{pmatrix} \mathbf{E}_\mathrm{p} & \mathbf{0} \\ \mathbf{0} & \mathbf{E} \end{pmatrix} \tag{43}$$

Differentiation with respect to λ leads to

$$\tilde{\mathbf{D}}\mathbf{\Phi}^\lambda + \tilde{\mathbf{D}}^\lambda\mathbf{\Phi} = \tilde{\mathcal{S}}\mathbf{\Phi}^\lambda\epsilon + \tilde{\mathcal{S}}^\lambda\mathbf{\Phi}\epsilon + \tilde{\mathcal{S}}\mathbf{\Phi}\epsilon^\lambda \tag{44}$$

which can be simplified by multiplication with $\Phi^\dagger$ from the left and using the normalization condition $\mathbf{\Phi}^\dagger\tilde{\mathcal{S}}\mathbf{\Phi} = \mathbf{I}$ to obtain

$$\mathbf{\Phi}^\dagger\tilde{\mathbf{D}}\mathbf{\Phi}^\lambda + \mathbf{\Phi}^\dagger\tilde{\mathbf{D}}^\lambda\mathbf{\Phi} = \mathbf{\Phi}^\dagger\tilde{\mathcal{S}}\mathbf{\Phi}^\lambda\epsilon + \mathbf{\Phi}^\dagger\tilde{\mathcal{S}}^\lambda\mathbf{\Phi}\epsilon + \epsilon^\lambda. \tag{45}$$

Introducing the matrix $\mathbf{O}^\lambda$ that describes the first-order orbital response with respect to perturbation λ

$$\mathbf{\Phi}^\lambda = \mathbf{\Phi}\mathbf{O}^\lambda, \tag{46}$$

and performing some mathematical rearrangements, one obtains[99]

$$\mathbf{O}^\lambda\epsilon - \epsilon\mathbf{O}^\lambda + \epsilon^\lambda = \mathbf{\Phi}^\dagger\tilde{\mathbf{D}}^\lambda\mathbf{\Phi} - \mathbf{\Phi}^\dagger\tilde{\mathcal{S}}^\lambda\mathbf{\Phi}\epsilon \tag{47}$$

from which the matrix elements of $\mathbf{O}^\lambda$ can be derived. ZFC showed that the response of the large and small components of the electronic states causes a mixing with the positronic states according to

$$\mathbf{A}^\lambda = \mathbf{A}_\mathrm{p}\mathbf{O}_2^\lambda + \mathbf{A}\mathbf{O}_4^\lambda = \mathbf{A}_\mathrm{p}\mathbf{O}_\mathrm{pe}^\lambda + \mathbf{A}_\mathrm{e}\mathbf{O}_\mathrm{ee}^\lambda \tag{48}$$

$$\mathbf{B}^\lambda = \mathbf{B}_\mathrm{p}\mathbf{O}_2^\lambda + \mathbf{B}\mathbf{O}_4^\lambda = \mathbf{B}_\mathrm{p}\mathbf{O}_\mathrm{pe}^\lambda + \mathbf{B}_\mathrm{e}\mathbf{O}_\mathrm{ee}^\lambda \tag{49}$$

where the subscripts e (electronic) and p (positronic) have been used to simplify the identification of mixed positronic–electronic contributions. By differentiation of $\mathbf{B}_\mathrm{e} = \mathbf{U}\mathbf{A}_\mathrm{e}$, one obtains

$$\frac{\partial\mathbf{U}}{\partial\lambda} = \left(\mathbf{B}_\mathrm{p}\mathbf{O}_\mathrm{pe}^\lambda - \mathbf{U}\mathbf{A}_\mathrm{p}\mathbf{O}_\mathrm{pe}^\lambda\right)\mathbf{A}_\mathrm{e}^\dagger\tilde{\mathbf{S}} \tag{50}$$

which can be directly calculated. Cheng and Gauss[101] neglected the contributions of the positronic wave function and kept only the last part of Eqs. (48) and (49). ZFC correctly included the positronic contributions and derived the full equation of the matrix $\mathbf{U}^\lambda$.[99]

Another important improvement of the calculation of the NESC gradient according to the procedure given by ZFC[92,99] resulted from the fact that these authors formulated the NESC first derivatives exclusively via traces of matrix products, in which the matrices of integral derivatives are contracted with precomputed square matrices. This saves time and disc space, as one does not need to recalculate the molecular integral derivatives or store them on disk. In particular, all terms of the first derivative of **G** and **U** were expressed in the form of traces of matrix products, which is more efficient compared to a term-by-term calculation and a final contraction of these terms with the respective integral derivatives.

NESC Calculations of Atomic Forces: Molecular Geometries

ZFC[92] used the analytical NESC energy gradient to determine molecular geometries. These authors found that only in the case of bond lengths between relativistic atoms an accurate account of the gradient of matrix **U** based on response theory is required, whereas in other cases an approximate calculation of $\partial\mathbf{U}/\partial\lambda$ is sufficient.[44] These authors calculated NESC/CCSD geometries for Hg-containing molecules and NESC/CCSD(T) bond dissociation energies (BDE) at NESC/CCSD geometries.

NESC/CCSD geometries were found to be reasonably close to experimental geometries (see HgCl and HgBr in Table 2). However, a final judgment on the accuracy of the NESC calculations could not be made because the influence of SOC on the bond length was not considered in their work.[44] Compared to other calculated values, NESC HgX bond lengths turned out to be closer to the experimental ones with deviations being smaller than 0.1 Å.[44] The agreement between NESC/CCSD(T) and experimental bond dissociation enthalpies (BDH) D_0 for mercury halides was excellent in view of a mean deviation of just 0.3 kcal mol^{-1}.[92]

A number of studies have been published since then, which confirm the reliability of NESC geometries either in connection with DFT or coupled cluster theory.[93–99]

TABLE 2 | NESC/CCSD Geometries and NESC/CCSD(T) Bond Dissociation Energies D_e (Enthalpies D_0) of Mercury Molecules[1]

Molecule	Symmetry	State	Method	Geometry Parameters	D_e (D_0)	Reference
HgF	$C_{\infty v}$	$^2\Sigma^+$	NESC/CCSD(T)//NESC/CCSD	2.024	33.0 (32.3)	92
			Expt.		32.9	116
HgCl	$C_{\infty v}$	$^2\Sigma^+$	NESC/CCSD(T)//NESC/CCSD	2.402	23.8 (23.4)	92
			SOC/ECP/CCSD(T)	2.354	22.9	117
			Expt.	2.395, 2.42	23.4, 24.6	118–120
HgBr	$C_{\infty v}$	$^2\Sigma^+$	NESC/CCSD(T)//NESC/CCSD	2.546	20.0 (17.5)	92
			SOC/ECP/CCSD(T)	2.498	16.3	117
			Expt.	2.62	17.2, 18.4	121–123
HgI	$C_{\infty v}$	$^2\Sigma^+$	NESC/CCSD(T)//NESC/CCSD	2.709	12.9 (7.6)	92
			SOC/ECP/CCSD(T)	2.708	8.6	117
			Expt.	2.81	7.8, 8.1, 8.9	119, 120, 124
HgCN	$C_{\infty v}$	$^2\Sigma^+$	NESC/CCSD(T)//NESC/CCSD	Hg–C: 2.118, C–N: 1.161	36.1	92
			IORA/QCISD	Hg–C: 2.114, C–N: 1.179		28, 125
HgNC	$C_{\infty v}$	$^2\Sigma^+$	NESC/CCSD(T)//NESC/CCSD	Hg–N: 2.077, N–C: 1.176	22.4	92
$HgCH_3$	C_{3v}	$^2A_1$	NESC/CCSD(T)//NESC/CCSD	Hg–C: 2.344, H–C: 1.084 Hg–C–H: 104.3	3.2	92

[1]From Ref 92. NESC/CCSD(T)//NESC/CCSD denotes NESC/CCSD(T) energies calculated at NESC/CCSD geometries. For HgX (X = F, Cl, Br, I), BDE values D_e include SOC corrections and are corrected by ZPE (zero-point energies) to yield D_0 values. In the calculations of $HgCH_3$, $HgOCH_3$, and $HgCF_3$, the fourteen 4f-electrons of Hg were frozen. D values in kcal mol^{-1}, bond lengths in Å, and angles in deg.

NESC Description of Molecular Density Distributions and Dipole Moments

The total electron density distribution $\rho(\mathbf{r})$ at a point $\mathbf{r}_P$ is the result of the response of a molecule to a perturbation λ that corresponds to the one-electron operator $\widehat{\delta}(\mathbf{r}_P - \mathbf{r})$, i.e., the Dirac delta operator. By using the Hellmann-Feynman theorem,[126,127] one gets

$$\left.\frac{\mathrm{d}E(\lambda)}{\mathrm{d}\lambda}\right|_{\lambda=0} = \left\langle \Psi \left| \widehat{\delta}(\mathbf{r}_P - \mathbf{r}) \right| \Psi \right\rangle = \rho(\mathbf{r}_P) \qquad (51)$$

When $\rho(\mathbf{r})$ is expanded in terms of basis functions, Eq. (51) describes the response density:

$$\rho(\mathbf{r}_P) = \sum_{\mu\nu} \tilde{\mathbf{P}}_{\mu\nu} \chi_\mu(\mathbf{r}_P) \chi_\nu(\mathbf{r}_P) \qquad (52)$$

Using the definition of the NESC gradient, the NESC response density matrix is given by $\tilde{\mathbf{P}} = \mathbf{GPG}^\dagger$ (see Eq. 29). Hence, the NESC electron density distribution can be written in terms of a renormalized matrix $\tilde{\mathbf{P}}$ depending on $\mathbf{P} = \mathbf{CnC}^\dagger$ where $\mathbf{C}$ is the matrix of the NESC orbital coefficients in the spin-free (scalar relativistic) 1-component representation. Once $\tilde{\mathbf{P}}$ is determined, the NESC electron density distribution can be calculated according to Eq. (52).

The difference density distribution

$$\Delta\rho(\mathbf{r})^{\mathrm{NESC}} = \rho(\mathbf{r})^{\mathrm{NESC}} - \rho(\mathbf{r})^{\mathrm{non\text{-}relat}} \qquad (53)$$

reveals how scalar relativistic effects lead to a change in the electron density distribution. For example, in Figure 2 the NESC difference density distribution of the molecule HAt is shown. Around the astatine atom a somewhat distorted pattern of spherical shells with density increase (red contour lines) and density depletion (blue lines) is recognizable. The shell structure is a result of the s,p-orbital contraction and d,f-orbital expansion, which propagates from the innermost core to the valence shell and which leads to a charge transfer from H to At. Because of the scalar relativistic effects the electronegativity of At increases.

The NESC density matrix has to be available when calculating NESC-based first-order response properties such as the molecular dipole moment or other electric multipole moments. In a static homogeneous electric field $\mathcal{F}$, the potential $V'(\mathbf{r})$ adopts the form

$$V'(\mathbf{r}) = V(\mathbf{r}) + \boldsymbol{\mathcal{F}} \cdot \mathbf{r} \qquad (54)$$

and the total molecular energy can be expressed in the form of a Taylor expansion according to

$$E(\boldsymbol{\mathcal{F}}) = E(0) + \frac{\partial E(\boldsymbol{\mathcal{F}})}{\partial \boldsymbol{\mathcal{F}}}|_{\boldsymbol{\mathcal{F}}=0} \cdot \boldsymbol{\mathcal{F}} + \frac{1}{2}\boldsymbol{\mathcal{F}} \cdot \frac{\partial^2 E(\boldsymbol{\mathcal{F}})}{\partial \boldsymbol{\mathcal{F}}\, \partial \boldsymbol{\mathcal{F}}}|_{\boldsymbol{\mathcal{F}}=0} \cdot \boldsymbol{\mathcal{F}} + \cdots \qquad (55)$$

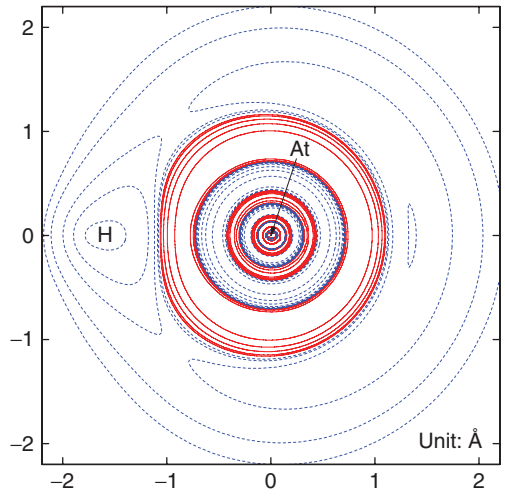

FIGURE 2 | Contourline diagram of the NESC difference density distribution of the HAt molecule. Solid red (dashed blue) contour lines indicate an increase (decrease) of the density because of scalar relativistic effects. The difference density adopts a shell structure at the At atom, which is caused by sp contraction. The outer red sphere corresponds to the 6s6p shell and and the most inner red sphere to the overlapping 3s3p and 2s2p shells. The 1 s region cannot be seen because it is just 0.1 Å outside the At nucleus. NESC/PBE0 calculations.

The first-order term of the expansion gives the electric dipole moment

$$\boldsymbol{\mu} = -\frac{\partial E(\boldsymbol{\mathcal{F}})}{\partial \boldsymbol{\mathcal{F}}}|_{\boldsymbol{\mathcal{F}}=0} \tag{56}$$

where the scalar dipole moment is defined as the norm of the dipole moment vector $\mu = ||\boldsymbol{\mu}||$.

Hence, the derivative of the electronic energy (24) has to be taken with regard to the components $\mathcal{F}_\alpha(\alpha = x, y, z)$ of the electric field. The only nonrelativistic contributions arise from $\mathbf{V}$; however, for NESC contributions from $\mathbf{W}$, $\mathbf{G}$, and $\mathbf{U}$ (since $\mathbf{G}$ depends on $\mathbf{U}$, and $\mathbf{U}$ depends on $\mathbf{V}$ and $\mathbf{W}$) also result. For component μ_α of the dipole moment one obtains:

$$\begin{aligned}\mu_\alpha &= -\mathrm{tr}\left[\mathbf{P}\frac{\partial \mathbf{H}_{1-e}}{\partial \mathcal{F}_\alpha}\right] = -\mathrm{tr}\left[\mathbf{P}\frac{\partial}{\partial \mathcal{F}_\alpha}\left(\mathbf{G}^\dagger \tilde{\mathbf{L}}\,\mathbf{G}\right)\right] \\ &= -\mathrm{tr}\left[\tilde{\mathbf{P}}\frac{\partial \tilde{\mathbf{L}}}{\partial \mathcal{F}_\alpha}\right] + \mathrm{tr}\left[\mathbf{D}\frac{\partial \mathbf{G}^\dagger}{\partial \mathcal{F}_\alpha} + \mathbf{D}^\dagger \frac{\partial \mathbf{G}}{\partial \mathcal{F}_\alpha}\right]\end{aligned} \tag{57}$$

ZFC[95] analyzed the individual terms of Eq. (57) and showed that, by eliminating small terms, it can be simplified to

$$\mu_\alpha = -\mathrm{tr}\left[\tilde{\mathbf{P}}\frac{\partial \tilde{\mathbf{L}}}{\partial \mathcal{F}_\alpha}\right] = -\mathrm{tr}\left[\tilde{\mathbf{P}}\frac{\partial \mathbf{V}}{\partial \mathcal{F}_\alpha}\right] \tag{58}$$

TABLE 3 | NESC/CCSD(T) and NESC/PBE0 Dipole Moments of Diatomic Molecules in Their Ground State Compared with Other Theoretical Values.[95]

Molecule	State	Method	R_e (Å)	μ (Debye)
AuF	$^1\Sigma^+$	NESC/CCSD(T)	[1]	4.32
		RECP/CCSD(T)/CBS[128]	[1]	4.37
		Expt.[129,130]	1.918	4.13
AuCl	$^1\Sigma^+$	NESC/CCSD(T)	[1]	3.81
		RECP/CCSD(T)/CBS[128]	[1]	3.90
		Expt.[131]	2.199	
AuBr	$^1\Sigma^+$	NESC/CCSD(T)	[1]	3.50
		RECP/CCSD(T)/CBS[128]	[1]	3.48
		Expt.[131]	2.318	
AuI	$^1\Sigma^+$	NESC/CCSD(T)	[1]	3.16
		RECP/CCSD(T)/CBS[128]	[1]	2.94
		Expt.[131]	2.506	
AuH	$^1\Sigma^+$	NESC/PBE0	1.530	1.47
		RECP/MP2[132]	1.51	1.03
		Expt.[116]	1.524	
HgH	$^2\Sigma^+$	NESC/PBE0	1.747	0.37
		Expt. [133,134]	1.741	0.47
HgF	$^2\Sigma^+$	NESC/PBE0	2.039	3.69
HgCl	$^2\Sigma^+$	NESC/PBE0	2.403	3.84
		Expt.[118]	2.395	

[1] Calculated at the experimental bond length. The NESC/CCSD(T) bond lengths for AuX are: 1.922 (X = F); 2.219 (Cl); 2.333 (Br); 2.482 Å (I).

Equation (58) reveals that the NESC dipole moment can reliably be calculated by combining the nonrelativistic formula with the NESC density matrix $\tilde{\mathbf{P}}$.

In Table 3, NESC bond lengths and NESC dipole moments of some diatomic Au- and Hg-containing molecules are listed together with the available experimental values. For the gold halides, NESC/CCSD(T) dipole moments (calculated at CCSD(T) and experimental bond lengths) are close to RECP/ CCSD(T)/CBS values,[128] which were obtained at the CCSD(T) level using experimental bond lengths, numerical derivatives, relativistic effective core potentials (RECPs), and aug-cc-pVnZ ($n = 4,5$) basis sets to extrapolate to the complete basis set (CBS) limit. NESC/CCSD(T) reproduces the results of the latter calculations within 0.1–0.2 Debye while requiring less than 10% of the computer time needed for the RECP/CCSD(T)/CBS calculations. For a larger set of calculated dipole moments, ZFC[95] found that NESC predicts the experimental values with an accuracy of 0.2 Debye or better.

NESC Hyperfine Structure Constants

Atoms and molecules possessing unpaired electrons, i.e., radicals, are recognized by the hyperfine structure (HFS) of their electron spin resonance (ESR) and optical spectra.[135,136] The hyperfine structure of the spectra arises from the interaction between the unpaired electrons and the magnetic field generated by the magnetic moments of the nuclei with nonzero spin. A nonuniform magnetic field characterized by the magnetic induction $\mathcal{B}(\mathbf{r})$ and its associated vector potential $\mathcal{A}(\mathbf{r})$ according to $\mathcal{B}(\mathbf{r}) = \nabla \times \mathcal{A}(\mathbf{r})$ result from the magnetic nuclei in the molecule. The vector potential is given by

$$\mathcal{A}(\mathbf{r}) = \frac{1}{c^2}\sum_K \frac{\boldsymbol{\mu}_K \times (\mathbf{r} - \mathbf{R}_K)}{|\mathbf{r} - \mathbf{R}_K|^3} \tag{59}$$

where $\boldsymbol{\mu}_K$ is the magnetic moment of the nucleus K at position $\mathbf{R}_K$.

For radicals, the magnitude of the HFS constants $\mathcal{A}_K$ obtained from the ESR spectra is related to the spin density distribution and therefore characteristic of the electronic structure of a radical.[135,136] These HFS constants can be quantum mechanically determined via the hyperfine tensor $\mathcal{A}_K$, which is given by the derivative of the total energy with respect to the nuclear magnetic moment $\boldsymbol{\mu}_K$. Two contributions result, which are determined by the so-called *Fermi-contact operator* and the *spin-dipole operator*:

$$\left(\hat{h}_K^{\mathrm{FC}}(\mathbf{r})\right)_\alpha = \frac{4\pi}{3c^2}\delta(\mathbf{r} - \mathbf{R}_K)\,\hat{\sigma}_\alpha \tag{60}$$

$$\left(\hat{h}_K^{\mathrm{SD}}(\mathbf{r})\right)_\alpha = \frac{1}{2c^2}\left(3\frac{(\hat{\boldsymbol{\sigma}}\cdot(\mathbf{r} - \mathbf{R}_K))(\mathbf{r} - \mathbf{R}_K)_\alpha}{|\mathbf{r} - \mathbf{R}_K|^5} - \frac{\hat{\sigma}_\alpha}{|\mathbf{r} - \mathbf{R}_K|^3}\right) \tag{61}$$

where α again denotes the Cartesian components of a vector. As a result of the molecular motion in the gas phase and in solution, the anisotropic spin-dipole contribution averages to zero so that the *isotropic* HFS constants $\mathcal{A}_K^{\mathrm{iso}}$ are determined by the Fermi-contact contributions associated with operators (60).

For organic molecules, the measurement of HFS constants is routine whereas it is still a challenge for radicals containing relativistic atoms. In the latter case, the quantum chemical calculation of HFS constants is an important option provided three prerequisites are fulfilled: (1) The wave function used must satisfy the Hellmann-Feynman theorem;[126,127] (2) Correlation corrected *ab initio* methods or at least well-tuned XC-functionals of DFT methods are required to get reliable values; and (3) relativity has to be taken into account.

Filatov and Cremer[125] demonstrated that useful HFS constants could be obtained with an open-shell IORA formalism (for related relativistic investigations, see also the work of the Baerends group or Malkin's work[137,138]). In extension of their work, FZC[97] derived an approach for calculating HFS constants with the Dirac-exact NESC method starting either from an unrestricted HF or unrestricted KS wave function. They obtained for $\mathcal{A}_K^{\mathrm{iso}}$ the following equation:

$$\begin{aligned}\mathcal{A}_K^{\mathrm{iso}} &= -g_e g_K \mu_B \mu_K \langle S_z\rangle^{-1} \\ &\quad\times \sum_\sigma \mathrm{tr}\left(\tilde{\mathbf{P}}_T^\sigma \mathbf{H}_{K,z}^{\mathrm{FC}} + \frac{3}{4}\tilde{\mathbf{P}}_W^\sigma\left(\mathbf{W}\mathbf{T}^{-1}\mathbf{H}_{K,z}^{\mathrm{FC}} + \mathbf{H}_{K,z}^{\mathrm{FC}}\mathbf{T}^{-1}\mathbf{W}\right)\right) \\ &= -g_e g_K \mu_B \mu_K \langle S_z\rangle^{-1} \\ &\quad\times \mathrm{tr}\left(\tilde{\mathbf{P}}_T^s \mathbf{H}_{K,z}^{\mathrm{FC}} + \frac{3}{4}\tilde{\mathbf{P}}_W^s\left(\mathbf{W}\mathbf{T}^{-1}\mathbf{H}_{K,z}^{\mathrm{FC}} + \mathbf{H}_{K,z}^{\mathrm{FC}}\mathbf{T}^{-1}\mathbf{W}\right)\right)\end{aligned} \tag{62}$$

In Eq. (62), $\mathbf{H}_{K,\alpha}^{\mathrm{FC}}$ is the matrix of the operator (60). The constants g_e, g_K, μ_B, and μ_K are the electron and nuclear g-factors as well as the Bohr and nuclear magnetons, respectively. The quantity $\langle S_z\rangle$ is the expectation value of the z-component of the electron spin. Matrices $\tilde{\mathbf{P}}_T^\sigma$ and $\tilde{\mathbf{P}}_W^\sigma$ are similarly defined as in the closed shell case[44] only that they refer in the open-shell calculation to a specific spin σ. The matrices $\tilde{\mathbf{P}}_T^s$ and $\tilde{\mathbf{P}}_W^s$ are calculated by substituting the spin-density matrix $\mathbf{P}^s = \mathbf{P}^\alpha - \mathbf{P}^\beta$ in the respective expressions.[97]

The calculated relativistic corrections of the mercury HFS values can be as large as 15,000 MHz (HgF[97]) or, as in the case of the mercury cation, more than 30,000 MHz (13,734 MHz at UHF compared with 43,400 MHz obtained with NESC/UHF[97]). Equally important is the inclusion of correlation effects, which is reflected by the NESC/QCISD and NESC/CCSD values given in Table 4.[97] At this level of theory, $\mathcal{A}_{\mathrm{Hg}}^{\mathrm{iso}}$ values are in good agreement with experiment. With the exception of HgH and HgF molecules, the deviation of the calculated HFS constants from the corresponding experimental value is within a few percent. Inclusion of electron correlation leads to a contraction of the atomic inner shell electron spin-density toward the nucleus, thus increasing the HFS constant.[125] For HgF, this increase is counterbalanced by the increasing bond polarity, which withdraws spin-density from the 6 s-orbital of Hg, thus reducing the value of the HFS constant. A delicate balance between these effects can only be achieved by using correlated methods including connected 3-electron correlation effects.

TABLE 4 | Isotropic Hyperfine Structure Constants $\mathcal{A}^{iso}_{Hg}$ (in MHz) of the Mercury Atom in Hg-Containing Molecules Calculated at the NESC/CCSD and NESC/QCISD Levels of Theory Compared with the Corresponding Experimental Values[97]

Molecule	Exp.	NESC/QCISD	NESC/CCSD
HgH	6859[1];7198[2]	7446	7463
HgF	22,163[3]	20,929	20,558
HgCN	15,960[4]	15,948	16,135
$HgCH_3$	4921[5]	5299	5428
$HgCH_2CH_3$		3504	3623
HgAg	2723[6]	2967	2962

[1]Ref 139; measurement in Ne matrix.
[2]Ref 139; Ar matrix.
[3]Ref 140; Ar matrix.
[4]Ref 141; Ar matrix.
[5]Ref 142; Ne matrix.
[6]Ref 143.

Problematic in this connection is that measured values are often obtained for molecules embedded in inert gas matrices (see Table 4). As was pointed out by Filatov and Cremer,[125] the effect of the inert gas matrix can change the HFS constant as much as 6–10%. Reliable NESC constants obtained with highly correlated methods and large basis sets could make it possible to determine these matrix effects.

NESC Electric Field Gradients

An electric field gradient (EFG) at an atomic nucleus exists only if the charges surrounding the nucleus in question (i.e., the electron density distribution and the other nuclei in a molecule) generate an inhomogeneous electric field, which via its electric field gradient provides a sensitive measure of the local electronic structure.[144] The EFG can be accessed via the nuclear quadrupole interaction that can be measured by various experimental techniques including Mössbauer spectroscopy,[145] nuclear quadrupole resonance spectroscopy,[146,147] or perturbed angular correlations (PAC) of γ-ray spectroscopy.[148] The interpretation of the experimental spectroscopic data often requires high-level theoretical calculations to reveal the relationship between electronic structure and measured nuclear quadrupole interactions.[149] In this connection, the same requirements apply as those mentioned in connection with the analysis of the HFS constants. For example, Pernpointner et al.[150] demonstrated the importance of including relativistic and electron correlation effects in the quantum chemical calculations when computing reliable EFG values for heavy atoms. This was confirmed by Arcisauskaite et al.[151] in high-level 4-component calculations on a series of mercury compounds.

The interaction of the nuclear quadrupole moment (NQM) $Q_{\alpha\beta}$ with the EFG $\mathcal{V}_{\alpha\beta}$ at the site of the nucleus is described by Eq. (63),[144,152]

$$\hat{H}^{\text{int}} = \sum_{\alpha,\beta} Q_{\alpha\beta}\mathcal{V}_{\alpha\beta} \tag{63}$$

where the summation is carried out with respect to the Cartesian components α, β. The NQM tensor components are given by:

$$Q_{\alpha\beta} = \frac{eQ}{2I\,(2I-1)}\left(\frac{1}{2}\left(\hat{I}_\alpha\hat{I}_\beta + \hat{I}_\beta\hat{I}_\alpha\right) - \frac{1}{3}\delta_{\alpha\beta}I\,(I+1)\right) \tag{64}$$

where I and $\hat{I}_\alpha$ are the nuclear spin and the nuclear spin operator, respectively, and e is the elementary charge. For nuclei with $I = 1/2$, all components $Q_{\alpha\beta}$ of the NQM tensor vanish.

For a given nucleus, the EFG operator is defined as a second derivative of the electron–nucleus attraction operator $\hat{V}$ with regard to the Cartesian coordinates,

$$\hat{\mathcal{V}}_{\alpha\beta} = \left(\frac{\partial}{\partial x_\alpha}\frac{\partial}{\partial x_\beta} - \frac{1}{3}\delta_{\alpha\beta}\nabla^2\right)\hat{V} \tag{65}$$

which describes the interactions of the nucleus in question with electrons and other nuclei in the molecule. It is convenient to define the principal axis system (by diagonalization of the $\mathcal{V}_{\alpha\beta}$ tensor), in which the axes a, b, and c are labeled in a way that the diagonal components $\mathcal{V}_{aa}$, $\mathcal{V}_{bb}$, and $\mathcal{V}_{cc}$ satisfy the relation $|\mathcal{V}_{aa}| \le |\mathcal{V}_{bb}| \le |\mathcal{V}_{cc}|$. Then, the EFG tensor can be characterized by the principal value $\mathcal{V}_{cc}$ and the asymmetry parameter $\eta = (\mathcal{V}_{aa} - \mathcal{V}_{bb})/\mathcal{V}_{cc}$. In practice, the nuclear quadrupole coupling constant (NQCC) ν_Q[144,146,153] is used to interpret nuclear quadrupole resonance (NQR) and Mössbauer spectra:[145,147]

$$\nu_Q = \frac{eQ\,\langle\mathcal{V}_{cc}\rangle}{h} \tag{66}$$

Here, $\langle\mathcal{V}_{cc}\rangle$ is the expectation value of the component $\mathcal{V}_{cc}$ in the ground state of the molecule.

The elements of the EFG tensor can be directly calculated as response properties. This is based on the fact that for any method satisfying the Hellmann-Feynman theorem,[126,127] the expectation value of an operator perturbing the Hamiltonian can be determined by differentiating the total energy of the perturbed system with respect to the perturbation parameter(s). In case of the NESC EFG at the position of nucleus K, one obtains the perturbed

TABLE 5 | Electric Field Gradients $\mathcal{V}_{cc}$ (in Atomic Units) Calculated for Hydrogen Halides HX (X = F, Cl, Br, I, At) Using the NESC/HF and NESC/MP2 Method with a Finite Size Nucleus Model[1]

Molecule	4c-DC-HF[2]	NESC/HF	NESC/MP2
HF	2.809754	2.809268	2.554123
HCl	3.591314	3.590261	3.402235
HBr	7.540289	7.536556	7.254653
HI	11.623332	11.620941	11.047529
HAt	25.979844	26.506524	26.273005

[1]From Ref 96.
[2]4-component Dirac–Coulomb Hartree–Fock calculations taken from Ref 154.

energy by adding the nuclear quadrupole interaction operator (63) to the potential energy operator of the NESC Hamiltonian and then differentiating the resulting total energy $E^{\mathrm{NESC}}\left(Q^K_{\alpha\beta}\right)$ with respect to the components of NQM $Q^K_{\alpha\beta}$:

$$\left\langle \mathcal{V}^K_{\alpha\beta} \right\rangle = \frac{\partial E^{\mathrm{NESC}}\left(Q^K_{\alpha\beta}\right)}{\partial Q^K_{\alpha\beta}}\Big|_{Q^K_{\alpha\beta}\to 0} + \sum_{L\neq K} Z_L \frac{3X_{\alpha,KL}X_{\beta,KL} - \delta_{\alpha\beta}R^2_{KL}}{R^5_{KL}} \tag{67}$$

where the second term on the r.h.s. represents the nuclear–nuclear part of the EFG and $X_{\alpha,KL}$ are the Cartesian components of the internuclear distance vector $\mathbf{R}_{KL} = \mathbf{R}_K - \mathbf{R}_L$. According to FZC,[96] the first term on the r.h.s. of Eq. (67) is given by

$$\frac{\partial E^{\mathrm{NESC}}\left(Q_{\alpha\beta}\right)}{\partial Q^K_{\alpha\beta}} = \mathrm{tr}\left[\tilde{\mathbf{P}} + \mathbf{P}_{0V} + (\mathbf{P}_{0V})^\dagger\right]\frac{\partial \mathbf{V}}{\partial Q^K_{\alpha\beta}} + \mathrm{tr}\left[\mathbf{U}\tilde{\mathbf{P}}\mathbf{U}^\dagger + \mathbf{P}_{0W} + (\mathbf{P}_{0W})^\dagger\right]\frac{\partial \mathbf{W}}{\partial Q^K_{\alpha\beta}} \tag{68}$$

where matrices $\tilde{\mathbf{P}}$, $\mathbf{P}_{0V}$, and $\mathbf{P}_{0W}$ are obtained from the usual molecular density matrix as described in Refs 92 and 97. Since no approximations are made in Eq. (68) the exact EFG is obtained.[96] The derivatives in Eq. (68) are formulated entirely in terms of traces of matrix products and the practical application of these formulae requires only a fraction of the time needed, e.g., for a single HF iteration.

FZC[96] investigated a series of molecules and found that with correlation corrected methods such as NESC/MP2 (second-order Moller-Plesset perturbation) accurate EFG values were obtained (see Table 5).

NESC Quadrupole Coupling Constants and the Nuclear Volume

A nonspherical distribution of the nuclear charge leads to an NQM Q.[144] Although the NQM plays an important role in nuclear physics and molecular spectroscopy, its direct experimental measurement is difficult and, currently, the most reliable way of its determination is based on measurement of an NQCC ν_Q in connection with accurately calculated EFGs $\mathcal{V}_{cc}$ (compare with Eq. 66):

$$Q = \nu_Q \frac{h}{e}\frac{1}{< \mathcal{V}_{cc} >} \tag{69}$$

where in the case of diatomic molecules $< \mathcal{V}_{cc} >= < \mathcal{V}_{zz} >$ with z corresponding to the molecular axis. The NQM and NQCC of two isotopes of the same element with atomic number Z can differ. The molecular NQCC includes a number of contributions which were analyzed in detail by Pyykkö.[155] Thus it was predicted that, in molecules with closed electronic shells, the variation of the nuclear volume in isotopes $I1$ and $I2$ of a given element Z should lead to the emergence of a *quadrupole anomaly* ${}^{I1}\Delta^{I2}_Z$, which, by analogy with the hyperfine anomaly, can be defined according to Eq. (70).

$$\frac{\nu_Q\,(I1)}{\nu_Q\,(I2)} = \frac{Q_{I1}}{Q_{I2}}\left(1 + {}^{I1}\Delta^{I2}_Z\right) \tag{70}$$

FZC[156] investigated the quadrupole anomaly by expanding the EFG of linear molecules at the position of an isotopic nucleus $I1$ in terms of the rms nuclear charge radius $< R_K > = a$:

$$\frac{\nu_Q\,(I1)}{\nu_Q\,(I2)} = \frac{Q_{I1}}{Q_{I2}}\frac{\mathcal{V}_{zz}\,(a_2) + (\partial \mathcal{V}_{zz}/\partial a)|_{a=a_2}\,(a_1 - a_2) + \ldots}{\mathcal{V}_{zz}\,(a_2)} = \frac{Q_{I1}}{Q_{I2}}\left(1 + \frac{1}{\mathcal{V}_{zz}}\left.\frac{\partial \mathcal{V}_{zz}}{\partial a}\right|_{a=a_2}\Delta a_{12} + O\left(\Delta a^2_{12}\right)\right) \tag{71}$$

In Eq. (71), the rms nuclear charge radius is given by a and the expansion is truncated at first order in a in view of its small variation between different isotopes. Thus, one can evaluate the magnitude of the quadrupole anomaly ${}^{I1}\Delta^{I2}_Z$ as the second term of the expansion given in parentheses in Eq. (71). By defining a relative quadrupole anomaly ${}^{I1}\delta^{I2}_Z$ as the difference between the ${}^{I1}\Delta^{I2}_Z$ values of two different molecules, $M1$ and $M2$, they obtained an expression that depended only on the EFG principal component

in the z-direction and its derivative with respect to a:[156]

$$
\begin{aligned}
{}^{I1}\delta_Z^{I2} &= {}^{I1}\Delta_Z^{I2}|_{M1} - {}^{I1}\Delta_Z^{I2}|_{M2} \\
&= \frac{Q_{I2}}{Q_{I1}}\left(\left.\frac{\nu_Q(I1)}{\nu_Q(I2)}\right|_{M1} - \left.\frac{\nu_Q(I1)}{\nu_Q(I2)}\right|_{M2}\right) \\
&\approx \left(\left(\frac{1}{\mathcal{V}_{zz}}\left.\frac{\partial \mathcal{V}_{zz}}{\partial a}\right|_{a=a_2}\right)_{M1}\right. \\
&\quad \left. - \left(\frac{1}{\mathcal{V}_{zz}}\left.\frac{\partial \mathcal{V}_{zz}}{\partial a}\right|_{a=a_2}\right)_{M2}\right)\Delta a_{12} \qquad (72)
\end{aligned}
$$

where Δa_{12} is the variation of the rms nuclear charge radius between the isotopes $I1$ and $I2$ of element Z.

The NESC/CCSD values of FZC for the relative quadrupole anomaly ${}^{195}\delta_{\mathrm{Au}}^{197}$ for pairs of gold molecules reached values large enough to be reflected by the measured by NQCC values. Thus, the NQCC ratio $\nu_Q\left({}^{195}_{79}\mathrm{Au}\right)/\nu_Q\left({}^{197}_{79}\mathrm{Au}\right)$ for AuCl referenced to other gold molecules gave the largest magnitude of the quadrupole anomaly, far above the precision of microwave spectroscopy, and by this provided a way of measuring changes in the nuclear volume for a variation from ${}^{195}_{79}\mathrm{Au}$ to ${}^{197}_{79}\mathrm{Au}$ ($a = 5.43439\,\mathrm{fm}$[111]).

NESC Contact Densities and Mössbauer Shifts

The Mössbauer effect involves the recoil-free emission and absorption of γ-radiation by atomic nuclei which are embedded in a solid environment.[157] The frequency of the resonant γ-radiation depends on the electronic environment of the resonating nucleus which is reflected by a frequency shift. To compensate for the corresponding frequency shift, the Doppler effect is used, which implies that the source of the γ-radiation is accelerated through a range of velocities until the resulting small energy shift reestablishes the resonance condition for the absorbing nucleus. The *isomer shift* δ is a measure for the electronic environment of the absorbing nucleus.[158,159] It can be expressed as

$$\delta = \alpha\left(\overline{\rho}^{(a)} - \overline{\rho}^{(s)}\right) \qquad (73)$$

where δ (in $\mathrm{mm\,s^{-1}}$) is given by the electron contact densities $\overline{\rho}$ at the position of the absorbing (a) and source (s) nucleus (in $\mathrm{bohr^{-3}}$) and α is a calibration constant depending on details of the nuclear γ-transition. Typically, α is determined by a linear regression analysis of the quantum chemically calculated contact densities against the experimental values of the isomer shifts.[145,160] Mössbauer isomer shifts have been measured for samples containing iron (^{57}Fe), tin (^{119}Sn), zinc (^{67}Zn), gold (^{197}Au), mercury (^{199}Hg and ^{201}Hg), and many rare earth elements (e.g., ^{151}Eu).[145,160–163]

Upon absorbing the γ-radiation, the a-nucleus undergoes a γ-transition, which leads to a change of the radius R of the a-nucleus and, by this, to a change in the electron–nucleus attraction potential, which depends on R_a. Filatov[164] suggested the use of linear response theory to calculate the isomer shift δ (and $\overline{\rho}$) as the electronic energy derivative with respect to the nuclear charge radius R_a of the a-nucleus:

$$\delta = \frac{c}{E_\gamma}\left(\left.\frac{\partial E^{\mathrm{a}}(R)}{\partial R}\right|_{R=R_a} - \left.\frac{\partial E^{\mathrm{s}}(R)}{\partial R}\right|_{R=R_a}\right)\Delta R_a \qquad (74)$$

where E^{a} and E^{s} denote the electronic energy of the absorbing and source systems, respectively.

A fully analytic approach for obtaining effective contact densities $\overline{\rho}$ within the linear response formalism based on NESC was presented by FZC.[98] Assuming a nuclear charge distribution according to Eq. (25), the nuclear attraction potential adopts the form given in Eq. (26), where the exponent ζ is related to the nuclear charge radius R_a of the a-nucleus by Eq. (27). Utilizing these equations, the effective contact density is obtained as[160,164]

$$\overline{\rho}_a = \frac{1}{2\pi}\frac{1}{Z_a\zeta}\left.\frac{\partial E(\zeta)}{\partial \zeta}\right|_{\zeta=\zeta_0} \qquad (75)$$

in which ζ_0 is the value of the parameter obtained from the experimentally measured rms charge radius of the resonating nucleus a. The effective contact density can be directly compared to the NESC density calculated as the expectation value of the density operator and used in connection with Eq. (73).[98,160,164]

FZC[98] calculated the derivatives of molecular integrals with respect to the nuclear charge radius or with respect to the parameter ζ of the Gaussian charge distribution given in Eq. (25), used the NESC response formalism for first-order properties, and obtained the effective contact density $\overline{\rho}_a$ at a specific nucleus a. These authors investigated the contact densities (in $\mathrm{e\,bohr^{-3}}$) of mercury as a free atom or bonded in a molecule, where in the latter case contact density differences $\overline{\rho}_{\mathrm{Hg}} - \overline{\rho}_{\mathrm{mol}}$ were determined (see Table 6).[98] Trends in the calculated contact density differences were reasonably reproduced already at the NESC/HF and NESC/MP2 levels of theory, although NESC/CCSD densities were the most reliable values.[98]

The values of the contact density difference are large when the electronic environment strongly differs

TABLE 6 | Effective Contact Densities (e bohr^{-3}) of the Hg Atom Obtained at the NESC Level of Theory

Atom/Molecule	NESC/HF	NESC/MP2	NESC/CCSD
Hg	2,104,944.971	2,105,047.821	2,105,035.382
Hg^{+}	112.876	127.943	121.136
Hg^{2+}	278.394	305.695	293.217
HgF	98.086	81.294	76.872
HgF_2	121.352	108.368	104.387
HgF_4	96.586	109.453	96.264
$HgCl_2$	108.118	94.572	91.592
$Hg(CH_3)_2$	49.001	43.610	42.184
$Hg(H_2O)_6^{2+}$	240.820	245.550	237.066

The absolute contact density is given for Hg($^1S_0$), whereas contact density difference values $\bar{\rho}_{Hg} - \bar{\rho}_{mol}$ are listed for ions and molecules.[97]

from that of the free Hg atom. The differences stretch from about 40 e bohr^{-3} in dimethyl mercury to 293 e bohr^{-3} in the mercury dication. With increasing electronegativity of the Hg-substituents, the difference contact density increases to 104 e bohr^{-3}, which confirms that the isomer shifts δ of Mössbauer spectroscopy reliably describe the environment of the Hg nucleus.[98]

SECOND-ORDER RESPONSE PROPERTIES

The analytical calculation of the energy Hessian with respect to external perturbations such as the displacement of the nuclear coordinates, the components of the electric field, or other quantities, is a prerequisite for obtaining second-order response properties of a molecule (vibrational frequencies, electric polarizabilities, infrared intensities, etc.). It is also one of the criteria when assessing the general applicability of a new quantum chemical method.[113] The eigenvalues of the Hessian matrix of second derivatives of the molecular energy with respect to the nuclear coordinates are used to characterize the nature of a stationary point obtained on the potential energy surface (PES) via optimization of the molecular energy, so that one can distinguish between minima, first-order and higher-order saddlepoints of the PES. Furthermore, they determine the curvature of a PES at a stationary point and by this the vibrational force constants of a molecule, which, by solving the basic equation of vibrational spectroscopy, lead to the molecular vibrational frequencies in their harmonic approximation.[165] These in turn are needed to calculate zero-point energies and vibrational contributions to the enthalpy and entropy at a given temperature.

The quantum chemical calculation of second-order response properties with nonrelativistic methods is a widely used standard procedure.[113] However, there is less computational data available for molecules containing relativistic atoms because in this case reliable methods have to be applied, which include both correlation and relativistic corrections.[1,13,14] The complexity of the full 4-component relativistic formalism restricts the reliable calculation of molecular properties to atoms and small molecules.[166–169] This makes the use of Dirac-exact methods such as NESC particularly attractive.

In the following, we will present the basic theory of calculating second-order response properties, which requires a derivation of the analytical second derivatives of the electronic energy with respect to a parameter λ. With the help of the analytical energy gradient of Eq. (28), the analytical second derivatives of E can be calculated according to

$$\begin{aligned}\frac{\partial^2 E}{\partial\mu\partial\lambda} &= \mathrm{tr}\left[\mathbf{\Omega}\frac{\partial^2\mathbf{S}}{\partial\mu\partial\lambda}\right] + \mathrm{tr}\left[\mathbf{P}\frac{\partial^2\mathbf{H}_{1-e}}{\partial\mu\partial\lambda}\right] \\ &+ \frac{1}{2}\mathrm{tr}\left[\mathbf{P}\frac{\partial^{2'}}{\partial\mu\partial\lambda}(\mathbf{J}-\mathbf{K})\right] + \mathrm{tr}\left[\frac{\partial\mathbf{\Omega}}{\partial\mu}\frac{\partial\mathbf{S}}{\partial\lambda}\right] \\ &+ \mathrm{tr}\left[\frac{\partial\mathbf{P}}{\partial\mu}\frac{\partial\mathbf{H}_{1-e}}{\partial\lambda}\right] + \frac{1}{2}\mathrm{tr}\left[\frac{\partial\mathbf{P}}{\partial\mu}\frac{\partial'}{\partial\lambda}(\mathbf{J}-\mathbf{K})\right] \end{aligned} \quad (76)$$

There are six contributions of which two (terms 1 and 3) can be directly determined utilizing standard nonrelativistic methods.[113] Contributions 4, 5, and 6 require either $\partial\mathbf{P}/\partial\mu$ or $\partial\mathbf{W}/\partial\mu$ and can be calculated with the help of the coupled perturbed equations[113,170] using the gradient $\partial\mathbf{H}_{1-e}/\partial\mu$. The solution of the NESC coupled perturbed equations was published by ZFC.[99] Hence, the major problem is the derivation of the second derivatives of the one-electron part given by contribution 2. This in turn leads to second derivatives of the NESC Hamiltonian matrix $\tilde{\mathbf{L}}$ and the renormalization matrix $\mathbf{G}$, which can be simplified by deleting those terms that are of the order $O(c^{-4})$. The important terms of the second and the fifth contribution of Eq. (76) are given by

$$\begin{aligned}&\mathrm{tr}\left[\frac{\partial\mathbf{P}}{\partial\mu}\frac{\partial\mathbf{H}_{1-e}}{\partial\lambda}\right] + \mathrm{tr}\left[\mathbf{P}\frac{\partial^2\mathbf{H}_{1-e}}{\partial\mu\partial\lambda}\right] \\ &= \mathrm{tr}\left[\left(\mathbf{U}\tilde{\mathbf{P}} + \tilde{\mathbf{P}}\mathbf{U}^{\dagger} - \mathbf{U}\tilde{\mathbf{P}}\mathbf{U}^{\dagger}\right)\frac{\partial^2\mathbf{T}}{\partial\mu\partial\lambda}\right]\end{aligned}$$

$$
\begin{aligned}
&+\mathrm{tr}\left[\left(\mathbf{U}\tilde{\mathbf{P}}\mathbf{U}^{\dagger}\right)\frac{\partial^2\mathbf{W}}{\partial\mu\partial\lambda}\right]+\mathrm{tr}\left[\tilde{\mathbf{P}}\frac{\partial^2\mathbf{V}}{\partial\mu\partial\lambda}\right]\\
&+\mathrm{tr}\left[\frac{\partial\mathbf{P}}{\partial\mu}\left(\frac{\partial\mathbf{G}^{\dagger}}{\partial\lambda}\tilde{\mathbf{L}}\mathbf{G}+\mathbf{G}^{\dagger}\tilde{\mathbf{L}}\frac{\partial\mathbf{G}}{\partial\lambda}+\mathbf{G}^{\dagger}\frac{\partial\tilde{\mathbf{L}}}{\partial\lambda}\mathbf{G}\right)\right]\\
&+\mathrm{tr}\left[\left(\mathbf{D}\frac{\partial^2\mathbf{G}^{\dagger}}{\partial\mu\partial\lambda}+\mathbf{D}^{\dagger}\frac{\partial^2\mathbf{G}}{\partial\mu\partial\lambda}\right)\right]\\
&+\mathrm{tr}\left(\mathbf{P}\left[\left(\frac{\partial\mathbf{G}^{\dagger}}{\partial\mu}\frac{\partial\tilde{\mathbf{L}}}{\partial\lambda}+\frac{\partial\mathbf{G}^{\dagger}}{\partial\lambda}\frac{\partial\tilde{\mathbf{L}}}{\partial\mu}\right)\mathbf{G}\right.\right.\\
&\left.\left.+\mathbf{G}^{\dagger}\left(\frac{\partial\tilde{\mathbf{L}}}{\partial\lambda}\frac{\partial\mathbf{G}}{\partial\mu}+\frac{\partial\tilde{\mathbf{L}}}{\partial\mu}\frac{\partial\mathbf{G}}{\partial\lambda}\right)\right]\right) \qquad (77)
\end{aligned}
$$

In Eq. (77), the major contributions result from the first four terms on the r.h.s. Whenever highly accurate values of the Hessian matrix are not needed (for example, for the calculation of vibrational frequencies needed for thermochemical corrections), terms 5 and 6 can be neglected and term 4 approximated, thus significantly saving computer time and core memory.[99] As in the case of the analytical NESC gradient, an accurate calculation of the second derivatives of the one-electron part involves the accurate calculation of the second derivatives of **U** and **G**, where in the former case the application of response theory and the consideration of the positronic states of the D-Hamiltonian is mandatory as was discussed by ZFC.[99]

NESC Infrared Spectra: Vibrational Frequencies and Infrared Intensities

Using the formalism described above, NESC vibrational frequencies can be calculated in combination with any electron correlated nonrelativistic method for which second derivatives are available. This is the case for most methods.[113] Although the calculation of vibrational frequencies is important for the characterization of stationary points on the PES or the conversion of energies into enthalpies and free energies (see above), an obvious challenge of quantum chemistry is the prediction of infrared spectra in connection with the identification and structural description of unknown compounds containing relativistic atoms. For this purpose, one has to be able to calculate infrared intensities. Calculated infrared intensities are nowadays often the only source for reliable values of this property because absolute (rather than relative) infrared intensities are difficult to measure.[171] Therefore, absolute infrared intensities are only known for some small molecules in the gas phase, whereas most measured intensities are given relative to the most intensive infrared band.[171]

The infrared intensity Γ is a response property, which can be calculated if the analytical derivatives of the energy with regard to nuclear coordinates and the components of the electric field $\mathcal{F}_\alpha$ are available. Alternatively, one can express it in the form of derivatives of the components of the molecular dipole moment with respect to the normal coordinates according to Eq. (78):[171]

$$\Gamma_i = \left(8\pi^3 N_\mathrm{A} g/3hc\right)\left|\frac{\partial\boldsymbol{\mu}}{\partial\mathcal{Q}_i}\right|^2 \qquad (78)$$

Constant N_A is the Avogadro number, h the Planck constant, and $\mathcal{Q}_i$ a normal coordinate of degeneracy g. Usually, the dipole moment derivatives are calculated for Cartesian coordinates α, which leads to Eq. (79). There, the intensity of mode i is given as

$$\Gamma_i = \boldsymbol{\delta}_i^{\dagger}\,\boldsymbol{\delta}_i = \mathbf{l}_i^{\dagger}\left(\boldsymbol{\Delta}^{\dagger}\boldsymbol{\Delta}\right)\mathbf{l}_i \qquad (79)$$

$$\boldsymbol{\delta}_i = \boldsymbol{\Delta}\,\mathbf{l}_i \qquad (80)$$

where atomic units are used and Δ denotes the rectangular dipole moment derivative matrix of dimension $3\times 3N$ given in Cartesian coordinates. The mass-weighted vibrational normal mode vectors $\mathbf{l}_i$ are determined when solving the vibrational secular equation in Cartesian coordinates.[165]

The NESC infrared intensity is obtained by calculating the derivative of Eq. (57), i.e., the NESC dipole moment, with respect to an atomic coordinate X_n:[95]

$$
\begin{aligned}
\Delta_{\alpha,n} &= \mathrm{tr}\left[\tilde{\mathbf{P}}\frac{\partial^2\tilde{\mathbf{L}}}{\partial X_n\partial F_\alpha}\right]+\mathrm{tr}\left[\frac{\partial\mathbf{P}}{\partial X_n}\left(\mathbf{G}^{\dagger}\frac{\partial\tilde{\mathbf{L}}}{\partial F_\alpha}\mathbf{G}\right)\right]\\
&= \mathrm{tr}\left[\tilde{\mathbf{P}}\frac{\partial^2\mathbf{V}}{\partial X_n\partial F_\alpha}\right]+\mathrm{tr}\left[\frac{\partial\mathbf{P}}{\partial X_n}\left(\mathbf{G}^{\dagger}\frac{\partial\mathbf{V}}{\partial F_\alpha}\mathbf{G}\right)\right] \qquad (81)
\end{aligned}
$$

where again first and second derivatives of matrices **U** and **G** are neglected because they make negligible contributions to the infrared intensity.[95]

ZFC[95,99] calculated a number of infrared spectra using NESC/PBE0. In Table 7, geometries, vibrational frequencies, and infrared intensities are compared with experimental results, some of which were obtained in the solid state as indicated. The calculated vibrational frequencies are in reasonable agreement with the available experimental data considering the harmonic approximation and the fact that NESC/PBE0 gives the calculated bond lengths

TABLE 7 | Comparison of NESC/PBE0 Geometries (Distances in Å), Harmonic Vibrational Frequencies (cm^{-1}), and Infrared Intensities ($km\,mol^{-1}$) with the Corresponding Experimental Values Measured in the Gas or the Solid Phase[1]

Molecule (Sym.)	Method	Geometry	Frequency (Infrared Intensity, Mode Symmetry)
AuH ($C_{\infty v}$)	NESC/PBE0	Au–H: 1.530	2283.7 (14.7; σ^+)
	Expt.[116]	Au–H: 1.524	2305.0 (σ^+)
AuH_2^- ($D_{\infty h}$)	NESC/PBE0	Au–H: 1.652	773.8 (115.7; π_u), 1685.2 (1035.8; σ_u^+), 1994.9 (0; σ_g^+)
	Expt.[172]		1636.0 (σ_u^+)
AuH_4^- (D_{4h})	NESC/PBE0	Au–H: 1.631	776.4 (0; b_{2g}), 793.9 (66.6; e_u), 828.7 (42.3; a_{2u}), 843.1 (0; b_{2u})
			1780.6 (2318.0; e_u), 2113.7 (0; b_{1g}), 2118.1 (0; a_{1g})
	Expt.[172]		1676.4 (e_u)
AuF ($C_{\infty v}$)	NESC/PBE0	Au–F: 1.923	556.7 (52.3; σ^+)
	Expt.[129]	Au–F: 1.918	563.7 (σ^+)
AuF_2^- ($D_{\infty h}$)	NESC/PBE0	Au–F: 1.963	184.4 (25.0; π_u), 516.3 (0; σ_g^+), 548.1 (182.7; σ_u^+)
AuF_4^- (D_{4h})	NESC/PBE0	Au–F: 1.916	184.0 (0; b_{2u}), 217.7 (0; b_{2g}), 233.1 (25.8; a_{2u}), 253.8 (8.7; e_u)
			572.0 (0; b_{1g}), 597.1 (0; a_{1g}), 613.4 (383.9; e_u)
	Expt.(solid)[173]		230 (b_{2g}), 561 (b_{1g}), 588 (a_{1g})
ThO ($C_{\infty v}$)	NESC/PBE0	Th–O: 1.826	926.1 (245.7; σ^+)
	Expt.[174]	Th–O: 1.840	895.8 (σ^+)
Th_2O_2 (D_{2h})	NESC/PBE0	Th–O: 2.089	155.7 (4.8; b_{3u}), 192.7 (0; a_g), 373.1 (0; b_{3g}), 527.2 (35.2; b_{2u}),
		O–Th–O: 74.4	623.8 (297.9; b_{1u}), 633.9 (0; a_g)
	Expt.[175]		619.7 (b_{1u})
UF_6 (O_h)	NESC/PBE0	U–F: 1.994	139.1 (0; t_{2u}), 184.0 (51.7; t_{1u}), 199.3 (0; t_{2g}), 539.1 (0; e_g)
			629.4 (810.3; t_{1u}), 681.4 (0; a_{1g})
	Expt.[176,177]	U–F: 1.996	142 (t_{2u}), 186.2 (~38; t_{1u}), 202 (t_{2g}), 532.5 (e_g), 624 (750; t_{1u})
			667.1 (a_{1g})
OsO_4 (T_d)	NESC/PBE0	Os–O: 1.686	352.6 (22.4; t_2), 356.5 (0; e), 1031.9 (465.8; t_2), 1063.9 (0; a_1)
	Expt.[178,179]	Os–O: 1.711	322.7 (t_2), 333.1 (e), 960.1 (t_2), 965.2 (a_1)
$^{265}HsO_4$ (T_d)	NESC/PBE0	Hs–O: 1.757	316.1 (32.9; t_2), 335.2 (0; e), 1010.4 (463.2; t_2), 1056.2 (0; a_1)

[1]For details, see Ref 95, 99.

somewhat too long. In general, stretching frequencies are somewhat too large (due to the harmonic approximation), whereas bending frequencies are somewhat too small (due to the somewhat too long bond lengths).

In the case of UF_6, experimental absolute intensities are available.[177] The t_{1u}-symmetrical vibrational modes at 184 (exp.: 186) and 629 (exp.: 624) cm^{-1} with intensities of 52 (exp.: 38) and 810 (exp.: 750) $km\,mol^{-1}$ are in good agreement with the experimental values (see Table 7). ZFC[95] showed that according to their calculated infrared intensities the polarity of an AuX (X = Br, Cl, F) bond strongly influences the intensity of the AuX stretching vibration. The calculated NESC/PBE0 values of the intensity increased from 5.1 to 12.9 to 52.3 $km\,mol^{-1}$ in this series. For the corresponding series of anions $XAuX^-$, there is an increase from 35 to 70 to 183 $km\,mol^{-1}$ (σ_u^+-stretching mode) and from 6 to 17 to 25 $km\,mol^{-1}$ (π_u-bending mode). Apart from the fact that infrared intensities are essential for identifying unknown compounds via their infrared spectra, they are also useful for deriving effective atomic charges.[180]

NESC Static Electric Dipole Polarizabilities

Another second-order response property important for the elucidation of the electronic structure of atoms and molecules is the static electric dipole polarizability, henceforth called polarizability for brevity. When a molecule is exposed to an external electric field, the electric dipole moment reflects the separation of positive and negative charge in the molecule, whereas the polarizability measures the deformation of the electron density distribution of an atom or molecule.[181] Knowledge of atomic and molecular polarizabilities is important in many areas

of chemistry ranging from electronic and vibrational spectroscopy to molecular modeling, drug design, and nanotechnology. Especially for molecules containing relativistic atoms, measured values of polarizabilities are sparse, and therefore their reliable prediction with the help of relativistic quantum chemical methods is desirable.

The second-order term in the Taylor expansion given in Eq. (54) defines the polarizability tensor:

$$\boldsymbol{\alpha} = -\left.\frac{\partial^2 E(\boldsymbol{\mathcal{F}})}{\partial \boldsymbol{\mathcal{F}} \partial \boldsymbol{\mathcal{F}}}\right|_{\boldsymbol{\mathcal{F}}=0} \tag{82}$$

Rather than using the tensor $\boldsymbol{\alpha}$, one normally prefers to work with the scalar isotropic polarizability, which is given by the average of the trace of the polarizability tensor[181]

$$\overline{\alpha} = \frac{1}{3}\left(\alpha_{xx} + \alpha_{yy} + \alpha_{zz}\right) \tag{83}$$

and which is invariant with respect to coordinate transformations.

ZFC[95] derived the formulas for the NESC polarizability, which takes a relative simple form after deleting small contributions involving the derivatives of **W**, **U**, and **G**;

$$\begin{aligned}\alpha_{\alpha\beta} &= -\mathrm{tr}\left[\tilde{\mathbf{P}}\frac{\partial^2 \tilde{\mathbf{L}}}{\partial \mathcal{F}_\alpha \partial \mathcal{F}_\beta}\right] - \mathrm{tr}\left[\frac{\partial \mathbf{P}}{\partial \mathcal{F}_\alpha}\left(\mathbf{G}^\dagger \frac{\partial \tilde{\mathbf{L}}}{\partial \mathcal{F}_\beta}\mathbf{G}\right)\right] \\ &= -\mathrm{tr}\left[\tilde{\mathbf{P}}\frac{\partial^2 \mathbf{V}}{\partial \mathcal{F}_\alpha \partial \mathcal{F}_\beta}\right] - \mathrm{tr}\left[\frac{\partial \mathbf{P}}{\partial \mathcal{F}_\alpha}\left(\mathbf{G}^\dagger \frac{\partial \mathbf{V}}{\partial \mathcal{F}_\beta}\mathbf{G}\right)\right]\end{aligned} \tag{84}$$

Since **V** is a linear function of the external electric field (see Eq. 54), the second derivative of **V** in the first term on the r.h.s vanishes, and Eq. (84) simplifies to Eq. (85)

$$\alpha_{\alpha\beta} = -\mathrm{tr}\left[\frac{\partial \mathbf{P}}{\partial \mathcal{F}_\alpha}\left(\mathbf{G}^\dagger \frac{\partial \mathbf{V}}{\partial \mathcal{F}_\beta}\mathbf{G}\right)\right] \tag{85}$$

Hence, the scalar relativistic formula for the polarizability differs from the nonrelativistic calculation only by the fact that the derivative $\partial \mathbf{V}/\partial \mathcal{F}_\beta$ has to be renormalized by matrix **G**. The derivative of **P** has to be calculated via a coupled-perturbed approach.[99]

In view of the fact that scalar relativistic effects lead to a contraction of the s- and p-orbitals and to an expansion of the d- and f-orbitals and that the latter effect is normally weaker than the former, one can in general expect a decrease of the electric polarizability as long as atoms are considered. However, in molecules, the interplay between relativistic and electron correlation effects necessitates the use of accurate theoretical methods for explaining trends in a series of related molecules.[182] ZFC[95] investigated the change in the isotropic polarizability $\overline{\alpha}$ for Au- and Hg-containing molecules as well as a number of other molecules by using the NESC formalism. Some of their results are summarized in Table 8.[95]

The relativistic corrections for the isotropic polarizabilities are between −0.2 and −2.0 Å^3, and the largest effect is found for HgH ($\overline{\alpha}$: 5.83–7.86 = −2.03 Å^3, see Table 8). These trends can be related to the contraction of the 6 s-orbital of Hg, which dominates scalar relativistic effects of mercury compounds. An exception is found for HgF_2 where the 6 s-orbital contraction is balanced by the electron-withdrawing ability of two electronegative F atoms so that the relativistic and nonrelativistic isotropic polarizabilities (4.13 and 4.06 Å^3, Table 8) become comparable. Apart from this, the isotropic polarizability follows some general trends: (1) the $\overline{\alpha}$ values are larger for anions than for neutral molecules or cations; (2) they are larger for radicals than for closed shell systems (see, e.g., HgH and HgH_2: 5.46 vs 5.01 Å^3, Table 8); (3) they increase with increasing atomic volume, i.e., with each additional electronic shell; and (4) molecules with more electropositive atoms possess larger $\overline{\alpha}$ values than those with more electronegative atoms.

ZFC[95] compared the isotropic polarizability of osmium tetroxide, OsO_4, and hassium tetroxide, HsO_4, obtained at the NESC level with experimental or previously published values. They found that the NESC/MP2 value of the isotropic polarizability (8.23 Å^3) is in close agreement with the experimental value of 8.17 Å^3. NESC/MP2 also predicted that the isotropic polarizability of HsO_4 is somewhat larger (8.30 Å^3, Table 8) than that of OsO_4 in agreement with the expectation that with increasing number of electrons and a more electropositive central atom the polarizability increases.

The NESC/PBE0 results for $\overline{\alpha}$ of the group 8 tetroxides are more than 1 unit too small (OsO_4: 6.89 Å^3). In general, NESC/MP2 polarizabilities are more reliable than the NESC/PBE0 results for $\overline{\alpha}$, which means that DFT can only be used for considering general trends. NESC polarizabilities were found to help correct flawed experimental data.[95] For example, the measured isotropic polarizability of UF_6 was measured to be 12.5 Å^3,[184] which is far too large in view of a NESC/MP2 value of 8.03 Å^3 (Table 8). The value of $\overline{\alpha}(HgCl_2)$ was given in the literature[184] as 11.6 Å^3, whereas the calculated NESC/MP2 value is 8.60 Å^3.[95]

TABLE 8 | Polarizabilities (in Å^3) at Optimized Geometries as Obtained with NESC/MP2, NESC/PBE0, or Nonrelativistic (NR) Calculations

Molecule	Method	α_{xx}	α_{yy}	α_{zz}	$\overline{\alpha}$
AuH	NESC/MP2	5.05	5.05	6.01	5.37
AuH_2^-	NESC/MP2	7.01	7.01	9.34	7.79
AuH_4^-	NESC/MP2	9.85	9.85	6.38	8.69
AuF	NESC/MP2	4.12	4.12	4.91	4.38
AuF_2^-	NESC/MP2	5.34	5.34	6.30	5.66
AuF_4^-	NESC/MP2	7.52	7.52	4.34	6.46
UF_6	NESC/MP2	8.03	8.03	8.03	8.03
OsO_4	NESC/MP2	8.23	8.23	8.23	8.23 (8.17)[183]
HsO_4	NESC/MP2	8.30	8.30	8.30	8.30
HgH	NESC/PBE0	5.05	5.05	7.38	5.83
	NESC/MP2	4.56	4.56	7.27	5.46
	NR/PBE0	7.50	7.50	8.57	7.86
HgH_2	NESC/PBE0	4.31	4.31	6.77	5.13
	NESC/MP2	4.19	4.19	6.66	5.01
	NR/PBE0	5.23	5.23	7.29	5.91
HgH_4	NESC/PBE0	7.58	7.58	4.32	6.49
	NESC/MP2	7.55	7.55	4.28	6.46
	NR/PBE0	9.05	9.05	4.95	7.68
HgF	NESC/PBE0	4.37	4.37	6.53	5.09
	NESC/MP2	3.87	3.87	6.85	4.86
	NR/PBE0	6.35	6.35	6.65	6.45
HgF_2	NESC/PBE0	3.31	3.31	5.75	4.13
	NESC/MP2	3.33	3.33	5.89	4.18
	NR/PBE0	3.30	3.30	5.57	4.06
HgF_4	NESC/PBE0	7.35	7.35	3.39	6.03
	NESC/MP2	8.23	8.23	3.44	6.64
	NR/PBE0	8.92	8.92	3.38	7.08

Experimental values are given in parentheses for comparison.[95]

NESC AS A TWO-COMPONENT METHOD: SPIN-ORBIT COUPLING

The SOC effect causes a splitting of the orbital energy levels (especially the *p*-levels of heavy atoms) according to the *jj*-coupling scheme.[1,12–14,24,185–187] This affects the strength of the chemical bond in molecules with heavy atoms, reaction and activation energies,[94] ionization potentials and electron affinities, and many other spectroscopic properties. In addition, SOC can lead to dynamic phenomena such as spin symmetry-forbidden transitions in molecular spectra or intersystem crossings between molecular states with different multiplicity. The calculation of SOC with NESC requires a 2-component formulation (2cNESC) as it was originally developed by Dyall.[1,68]

FZC[103] developed a 2-component NESC method closely following Dyall's work.[68] This required the inclusion of the SOC operator, which is split into a one- and a two-electron part. For heavy elements, SOC is dominated by the one-electron term. The two-electron spin-orbit (SO) contributions often reduce the former term by about 5% for elements with a filled 5d shell and by about 10% in the case of elements with a filled 6d shell,[103] which is an indication of their overall screening effect. These contributions are not negligible, however, in most cases they are parallel to the one-electron SO terms.[188]

In view of the much smaller two-electron contributions and the significantly larger costs to calculate them,[189] FZC[103] estimated the magnitude of the two-electron part from the magnitude of the one-electron SO part, where the latter was accurately

determined. They employed the screened-nuclear-spin-orbit (SNSO) approach of Boettger,[190] which was originally formulated within the DKH quasi-relativistic approximation[49–51] and which had been used by several other authors.[191–193]

In the modified Dirac equation[1,68] given in Eq. (7), the matrix $\mathbf{W} = (\boldsymbol{\sigma} \cdot \mathbf{p}) V(\mathbf{r}) (\boldsymbol{\sigma} \cdot \mathbf{p}) / 4m^2c^2$ can be split into a spin-free (sf) and spin-dependent part according to Eq. (86):

$$\mathbf{W} = \mathbf{W}^{\mathrm{sf}} + i\boldsymbol{\sigma} \cdot \mathbf{W}^{\mathrm{SO}} \tag{86}$$

The separation is achieved by the use of the Dirac identity $(\boldsymbol{\sigma} \cdot \mathbf{A})(\boldsymbol{\sigma} \cdot \mathbf{B}) = \mathbf{A} \cdot \mathbf{B} + i\boldsymbol{\sigma} \cdot (\mathbf{A} \times \mathbf{B})$ and the sf and the SO parts of the $\mathbf{W}$ matrix are defined in Eq. (8).

$$\mathbf{W}^{\mathrm{sf}}_{\overline{\mu}\overline{\nu}} = -\left\langle \overline{\mu} \left| \frac{1}{4m^2c^2} \nabla \cdot V(\mathbf{r}) \nabla \right| \overline{\nu} \right\rangle \tag{87a}$$

$$\mathbf{W}^{\mathrm{SO}}_{\overline{\mu}\overline{\nu}} = -\left\langle \overline{\mu} \left| \frac{1}{4m^2c^2} \nabla \times V(\mathbf{r}) \nabla \right| \overline{\nu} \right\rangle \tag{87b}$$

In these equations, a spinor basis set $\overline{\chi}$ is used which comprises basis functions for both α and β spin. As pointed out above, the sf-NESC formalism is obtained by neglecting the SO part of the $\mathbf{W}$ matrix.[1,44] The inclusion of the spin-dependent part of $\mathbf{W}$ needed for SOC is still practical for large molecules as long as only the one-electron potential (i.e., the electron-nuclear attraction potential) has to be determined.[44]

By calculating just the one-electron part in Eq. (87b), SO splittings in many-electron systems are seriously overestimated. Including however the SNSO approximation,[14,190] the SOC terms of the one-electron NESC Hamiltonian are effectively scaled down so that reasonable SO splittings are obtained.[103] This is accomplished with the help of basis-function-dependent scaling factors, which simulate the effect of the missing two-electron SO terms:

$$\left(\mathbf{H}^{\mathrm{NESC}}_{\mathrm{1e,SNSO}}\right)_{\overline{\mu}\overline{\nu}} = \left(\mathbf{H}^{\mathrm{NESC}}_{\mathrm{1e,SO}}\right)_{\overline{\mu}\overline{\nu}} - \sqrt{\frac{Q\left(l_{\overline{\mu}}\right)}{Z_{\overline{\mu}}}} \left(\mathbf{H}^{\mathrm{NESC}}_{\mathrm{1e,SO}}\right)_{\overline{\mu}\overline{\nu}} \sqrt{\frac{Q\left(l_{\overline{\nu}}\right)}{Z_{\overline{\nu}}}} \tag{88}$$

In Eq. (88), $Z_{\overline{\mu}}$ is the charge of the nucleus at which the spinor basis function $\overline{\mu}$ is centered and $Q\left(l_{\overline{\mu}}\right)$ is a screening factor that depends on the orbital angular momentum of the function $\overline{\mu}$; in particular, $Q(l) = 0, 2, 10, 28, \cdots$ for $l = 0, 1, 2, 3, \cdots$. By further improving the SNSO approach (called modified SMSO or mSNSO), FZC[103] obtained for atoms with $1 \le Z \le 120$ and $l \le 6$ (i.e., *i*-type basis functions) an agreement of the calculated SO splittings within 0.02 hartree (spinors with $j \ge 7/2$) compared to 4-component DHF results. These authors used the 2-component NESC(SNSO) or NESC(mSNSO) approach in connection with the general HF (GHF) or general Kohn-Sham (GKS) formalism for obtaining the total energy and spinor energies of many-electron systems.[194–196]

The performance of NESC(SNSO) is illustrated in Figure 3 for spinor energy splittings of $Z = 120$ (Ubn: unbinilium) by plotting their deviation (in percentage) from exact splittings obtained with the 4-component DHF method.

The one-electron SO contributions (given in red) exaggerate calculated *n*p-splittings on the average by 2%, *n*d-splittings by 10%, and *n*f-splittings by 33% with the deviations becoming somewhat larger with increasing principal quantum number *n*. This exaggeration is largely corrected by the screened nucleus two-electron contributions so that final 2-component NESC(SNSO) values differ by just 2% from the Dirac values. After the mSNSO correction, the deviations are 1% for *n*p-splittings and only increase to 3% for the *n*f-splittings.[103]

This observation was confirmed when calculating the SO splitting of spinor energies in molecules.[103] In Table 9, calculated SO splittings in cm^{-1} are given for hydrogen halides HX (valence-shell *n*pπ splittings) with X = F, Cl, Br, I, At, Uus (ununseptium, $Z = 117$) and mercury(II) halides HgX_2 (mercury 5dπ and 5dδ splittings) with X = F, Cl, Br, I. For HX molecules, the splittings range from 380 to 23,955 cm^{-1}, with the NESC values always being somewhat larger (up to 60 cm^{-1}) indicating that they slightly exaggerate the splittings because of the approximate two-electron contributions to SOC. However, the deviations when given in percentage are similar to those found for atoms. In the case of HgX_2 molecules, the overall magnitude and the relative precision of the calculated SO splittings were of the same order of magnitude as for the bare Hg atom. FZC observed that with the 2-component NESC(mSNSO)/GHF approach reliable SO splittings and SOC corrections of relative energies can be calculated.[103]

CONCLUSIONS

The last two decades have seen a rapid development of relativistic 1-component and 2-component methods derived from the exact 4-component Dirac formalism. This was triggered by Dyall's 1997 article[68] on the NESC method and his development of programmable NESC equations. Although it needed more than

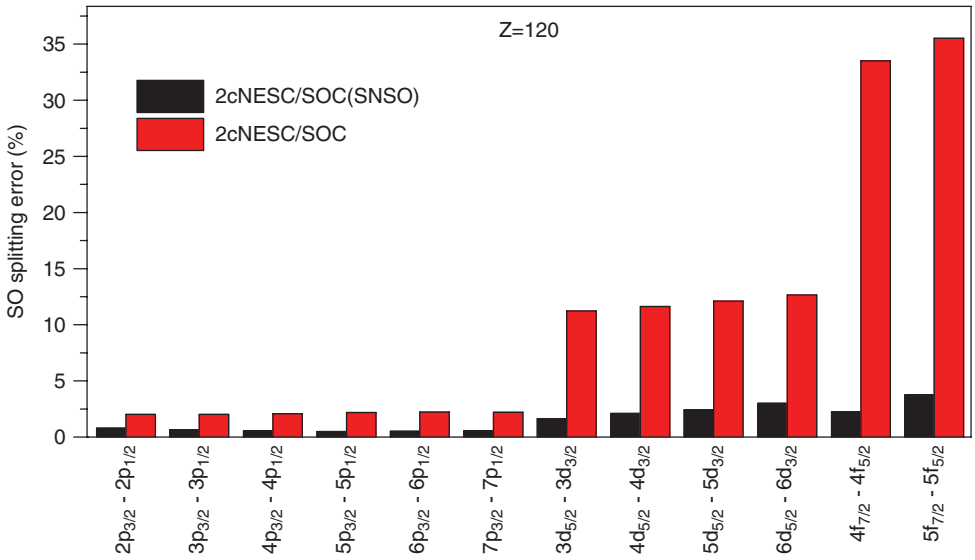

FIGURE 3 | Deviations (in percentage) of the 2-component (2c) NESC/SOC/GHF and NESC/SOC(SNSO)/GHF spinor energy splittings from exact 4-component DHF splittings given in the case $Z = 120$.

TABLE 9 | SO Splittings (in cm^{-1}) of the Valence np_π Orbitals of HX and the $5d_{\pi,\delta}$ Orbitals of HgX_2 as Given by 4-Component Dirac/HF and 2-Component NESC(mSNSO)/GHF Calculations, Both Obtained with a Finite Nucleus Model.[103]

Molecule	Splitting[1]	Dirac 4-Component	NESC(mSNSO) 2-Component
HF	$2p\pi_{3/2}$ - $2p\pi_{1/2}$	381	371(−2.6)
HCl	$3p\pi_{3/2}$ - $3p\pi_{1/2}$	758	762(0.5)
HBr	$4p\pi_{3/2}$ - $4p\pi_{1/2}$	2994	3025(1.0)
HI	$5p\pi_{3/2}$ - $5p\pi_{1/2}$	5942	5979(0.6)
HAt	$6p\pi_{3/2}$ - $6p\pi_{1/2}$	15513	15538(0.2)
HUus	$7p\pi_{3/2}$ - $7p\pi_{1/2}$	23955	23978(0.1)
HgF_2	$5d\pi_{3/2}$ - $5d\pi_{1/2}$	5362	5357(−0.5)
	$5d\delta_{5/2}$ - $5d\delta_{3/2}$	18769	19076(1.6)
$HgCl_2$	$5d\pi_{3/2}$ - $5d\pi_{1/2}$	16266	16579(1.9)
	$5d\delta_{5/2}$ - $5d\delta_{3/2}$	17613	17955(1.9)
$HgBr_2$	$5d\pi_{3/2}$ - $5d\pi_{1/2}$	16095	16415(2.0)
	$5d\delta_{5/2}$ - $5d\delta_{3/2}$	17446	17794(2.0)
HgI_2	$5d\pi_{3/2}$ - $5d\pi_{1/2}$	15196	15506(2.0)
	$5d\delta_{5/2}$ - $5d\delta_{3/2}$	17286	17637(2.0)

[1]Different ω-spinors with the same symmetry are differentiated by labeling them according to the dominant spin-free orbital. For Uus ($Z = 117$), a mass number of $2.556Z$ was used. Relative deviations (in %) from the 4-component Dirac/HF values are given in parentheses.

10 years to solve the NESC equations exactly with an algorithm that could also be applied to large molecules with thousands of basis functions,[44] Dyall's work represented directly or indirectly an instigator of work by Kutzelnigg and Liu,[45,76,77] Saue,[85] Reiher, Wolf, and Hess,[71–74] Barysz and Kedziera,[83,86] and many others. This was reflected by the development of the infinite-order DKH, the IOTC, or the X2C methods. Furthermore, Dyall's work was essential for a paradigm shift from an operator-driven to a matrix-driven development of relativistic quantum chemical methods.

Today the NESC method can be routinely applied in its spin-free, 1-component form to determine first-order response properties such as geometries, electron density distributions, electric moments, electric field gradients, hyperfine structure constants, contact densities and Mössbauer isomer shifts or nuclear quadrupole coupling constants, etc. Also, there is the possibility of determining in a standard manner second-order response properties such as vibrational frequencies and vibrational force constants in the harmonic approximation, static electric dipole polarizabilities, infrared intensities, magnetic shieldings, etc. Clearly, the repertoire of molecular properties which can be calculated with the NESC method will be successively extended in the near future, hopefully including properties such as anharmonic corrections to the vibrational frequencies or the indirect spin–spin coupling constants of nuclear magnetic resonance spectroscopy.

The usefulness and general applicability of 2-component NESC methods is also steadily growing. The calculation of SOC effects with the GHF method is surprisingly successful, although setbacks in the form of symmetry-breaking or variational problems will probably emerge. In this connection, one will need also more experience with both the GHF and

GKS method. The inclusion of analytical derivatives will be the next step in this development to routinely calculate SOC-corrected geometries and other first-order response properties.

NESC is built on the DC-Hamiltonian. Its extension to the DCB-Hamiltonian will be a challenge and necessity for molecules containing transactinides. Much work has been carried out in this connection, however easy applicable methods, which can be used for large basis set calculations and in connection with correlation corrected nonrelativistic methods, are not available. For highly accurate calculations, QED effects have to be considered. However, these challenges are outside the realm of chemistry where it is sufficient to achieve chemical accuracy (± 1 kcal mol^{-1}) rather than a spectroscopic accuracy of a few cm^{-1}.

In view of the challenges posted by the chemistry of heavy and superheavy elements, we foresee also for this decade an active and rapid development of new relativistic methods, for which Dirac-exact methods will provide a solid fundament. Apart from this, NESC will be the basis for numerous investigations on molecules and chemical reactions involving relativistic atoms, which will be facilitated once the computer programs based on NESC will become generally available.

ACKNOWLEDGMENTS

This work was financially supported by the National Science Foundation, Grant CHE 1152357. We thank SMU for providing excellent computational facilities.

REFERENCES

1. Dyall KG, Fægri K. *Introduction to Relativistic Quantum Chemistry*. Oxford: Oxford University Press; 2007.
2. Grant IP. *Relativistic Quantum Theory of Atoms and Molecules, Theory and Computation*. New York: Springer; 2007.
3. Reiher M, Wolf A. *Relativistic Quantum Chemistry, The Fundamental Theory of Molecular Science*. Weinheim: Wiley-VCH; 2009.
4. Pyykkö P. *Relativistic Theory of Atoms and Molecules, A Bibliography 1916–1985*. Lecture Notes in Chemistry, vol. 41. Berlin: Springer; 1986.
5. Pyykkö P. Relativistic effects in structural chemistry. *Chem Rev* 1988, 88:563.
6. Pyykkö P. *Relativistic Theory of Atoms and Molecules, A Bibliography 1986–1992*. Lecture Notes in Chemistry, vol. 60. Berlin: Springer; 1993.
7. Pyykkö P. *Lecture Notes in Chemistry*, vol. 76. Berlin: Springer; 2000.
8. Pyykkö P. The rtam electronic bibliography, version 17.0, on relativistic theory of atoms and molecules. *J Comput Chem* 2013, 34:2667.
9. Almlöf J, Gropen O. *Reviews in Computational Chemistry*, Vol. 8, Lipkowitz KB, Boyd DB. (ed.) JVCH Publishers, New York; 1996, 203–244.
10. Schwerdtfeger P, Seth M. *Encyclopedia of Computational Chemistry*, Vol. 4, Schleyer PVR, Allinger NL, Clark T, Gasteiger J, Kollman PA, Schaefer HF III, and Schreiner PR. John Wiley, Chichester (1998), 2480 .
11. Hess BA, Marian CM. In: Jensen P, Bunker PR, eds. *Computational Molecular Spectroscopy*. Sussex: Wiley; 2000, 152–278.
12. Liu W. Ideas of relativistic quantum chemistry. *Mol Phys* 2010, 108:1679.
13. Saue T. Relativistic Hamiltonians for chemistry: a primer. *Chem Phys Chem* 2011, 12:3077.
14. Peng D, Reiher M. Exact decoupling of the relativistic fock operator. *Theor Chem Acc* 2012, 131:1081.
15. Pyykkö P. Relativistic effects in chemistry: more common than you thought. *Ann Rev Phys Chem* 2012, 63:45.
16. Einstein A. On the electrodynamics of moving bodies. *Ann Phys* 1905, 17:891.
17. NIST. Codata internationally recommended values. 2010. Available at: http://physics.nist.gov/cgi-bin/cuu/Value?alphinv.
18. Pyykkö P. In: Löwdin P-O, ed. *Advances in Quantum Chemistry*, vol. 11. New York: Academic Press; 1978, 353–409.
19. Greenwood NN, Earnshaw A. *Chemistry of the Elements*. Oxford: Butterworth-Heinemann; 1997.
20. Porterfield WW. *Inorganic Chemistry, A Unified Approach*. San Diego: Academic Press; 1993.
21. Ziegler T, Snijders JG, Baerends EJ. On the origin of relativistic bond contraction. *Chem Phys Lett* 1980, 75:1.
22. Ziegler T, Snijders JG, Baerends EJ. Relativistic effects on bonding. *J Chem Phys* 1981, 74:1271.

23. Snijders JG, Pyykkö P. Is the relativistic contraction of bond lengths an orbital-contraction effect? *Chem Phys Lett* 1980, 75:5.
24. Marian CM. Spin-orbit coupling and intersystem crossing in molecules. *WIREs Comput Mol Sci* 2012, 2:187.
25. Christensen NE, Seraphin BO. Relativistic band calculation and the optical properties of gold. *Phys Rev B* 1971, 4:3321.
26. Romaniello P, de Boeij PL. The role of relativity in the optical response of gold within the time-dependent current-density-functional theory. *J Chem Phys* 2005, 122:164303.
27. Glantschnig K, Ambrosch-Draxl C. Relativistic effects on the linear optical properties of Au, Pt, Pb and W. *New J Phys* 2010, 12:103048.
28. Filatov M, Cremer D. Revision of the dissociation energies of mercury chalcogendies—unusual types of mercury bonding. *Chem Phys Chem* 2004, 121:1547.
29. Cremer D, Kraka E, Filatov M. Bonding in mercury molecules described by the normalized elimination of the small component and coupled cluster theory. *Chem Phys Chem* 2008, 9:2510.
30. Desclaux JP. Relativistic Dirac-Fock expectation values for atoms with atomic numbers z = 1 -120. *Atomic Data Nuclear Data Tables* 1973, 311:891.
31. Pyykkö P, Desclaux JP. Relativity and the periodic system of elements. *Acc Chem Res* 1979, 12:276.
32. Calvo F, Pahl E, Wormit M, Schwerdtfeger P. Evidence for low-temperature melting of mercury owing to relativity. *Angew Chem Int Ed Engl* 2013, 52: 7583.
33. Lamb WE, Retherford RC. Fine structure of the hydrogen atom by a microwave method. *Phys Rev* 1947, 72:241.
34. Feynman R. *QED: The Strange Theory of Light and Matter*. Princeton, NJ: Princeton University Press; 1985.
35. Pyykkö P, Tokman M, Labzowsky LN. Estimated valence-level Lamb shifts for group 1 and group 11 metal atoms. *Phys Rev A* 1998, 57:R689.
36. Pyykkö P. The physics behind chemistry and the periodic table. *Chem Rev* 2012, 112:371.
37. Dirac PAM. The quantum theory of the electron. *Proc R Soc Lond* 1928, A117:610.
38. Dirac PAM. Quantum mechanics of many-electron systems. *Proc R Soc Lond* 1929, A123:714.
39. Swirles B. The relativistic self-consistent field. *Proc R Soc Lond* 1935, A152:625.
40. Hafner P. The Kramers restricted Hartree-Fock approach. *J Phys B At Mol Phys* 1980, 13:3297.
41. Breit G. The effect of retardation on the interaction of two electrons. *Phys Rev A* 1929, 34:553.
42. Stanton RE, Havriliak S. Kinetic balance: a partial solution to the problem of variational safety in Dirac calculations. *J Chem Phys* 1984, 81:1910.
43. Dyall KG, Fægri K. Kinetic balance and variational bounds failure in the solution of the Dirac equation in a finite Gaussian basis set. *Chem Phys Lett* 1990, 174:25.
44. Zou W, Filatov M, Cremer D. An improved algorithm for the normalized elimination of the small-component method. *Theor Chem Acc* 2011, 130:633.
45. Liu W, Kutzelnigg W. Quasirelativistic theory. II. Theory at matrix level. *J Chem Phys* 2007, 126:114107.
46. Brown GE, Ravenhall DG. On the interaction of two electrons. *Proc R Soc Lond* 1951, A208:552.
47. Sucher J. Foundations of the relativistic theory of many-electron atoms. *Phys Rev A* 1980, 22:348.
48. Foldy LL, Wouthuysen SA. On the Dirac theory of spin 1/2 particles and its non-relativistic limit. *Phys Rev* 1950, 78:29.
49. Douglas M, Kroll NM. Quantum electrodynamical corrections to the fine structure of helium. *Ann Phys* 1974, 82:89.
50. Hess BA. Applicability of the no-pair equation with free-particle projection operators to atomic and molecular structure calculations. *Phys Rev A* 1985, 32:756.
51. Hess BA. Relativistic electronic-structure calculations employing a two-component no-pair formalism with external-field projection operators. *Phys Rev A* 1986, 33:3742.
52. Jansen G, Hess BA. Revision of the Douglas-Kroll transformation. *Phys Rev A* 1989, 39:6016.
53. Samzow R, Hess BA, Jansen G. The two-electron terms of the no-pair Hamiltonian. *J Chem Phys* 1992, 96:1227.
54. Nakajima T, Hirao K. The higher-order Douglas-Kroll transformation. *J Chem Phys* 2000, 113:7786.
55. van Wuellen C. Relation between different variants of the generalized Douglas-Kroll transformation through sixth order. *J Chem Phys* 2003, 120:7307.
56. Chang C, Pelissier M, Durand P. Regular two-component Pauli-like effective Hamiltonians in Dirac theory. *Phys Script* 1986, 34:394.
57. van Lenthe E, Baerends E-J, Snijders JG. Relativistic regular two-component Hamiltonians. *J Chem Phys* 1993, 99:4597.
58. van Lenthe E, Baerends EJ, Snijders JG. Relativistic total energy using regular approximations. *J Chem Phys* 1994, 101:9783.
59. van Lenthe E, Ehlers A, Baerends E-J. Geometry optimizations in the zero order regular approximation for relativistic effects. *J Chem Phys* 1999, 110:8943.

60. Dyall KG, van Lenthe E. Relativistic regular approximations revisited: an infinite-order relativistic approximation. *J Chem Phys* 1999, 111:1366.
61. Filatov M. On representation of the Hamiltonian matrix elements in relativistic regular approximation. *Chem Phys Lett* 2002, 365:222.
62. Filatov M, Cremer D. On the physical meaning of the Zora Hamiltonian. *Mol Phys* 2003, 101:2295.
63. Filatov M, Cremer D. Analytic energy derivatives for regular approximations of relativistic effects applicable to methods with and without correlation corrections. *J Chem Phys* 2003, 118:6741.
64. Filatov M, Cremer D. Calculation of electric properties using regular approximations to relativistic effects: the polarizabilities of RuO_4, OsO_4, and HsO_4 (z=108). *J Chem Phys* 2003, 119:1412.
65. Filatov M, Cremer D. Representation of the exact relativistic electronic Hamiltonian within the regular approximation. *J Chem Phys* 2003, 119:11526.
66. Filatov M, Cremer D. A gauge-independent zeroth-order regular approximation to the exact relativistic Hamiltonian-formulation and applications. *J Chem Phys* 2005, 122:044104.
67. Filatov M, Cremer D. Connection between the regular approximation and the normalized elimination of the small component in relativistic quantum theory. *J Chem Phys* 2005, 122:064104.
68. Dyall KG. Interfacing relativistic and nonrelativistic methods. I. Normalized elimination of the small component in the modified Dirac equation. *J Chem Phys* 1997, 106:9618.
69. Dyall KG, Enevoldsen T. Interfacing relativistic and nonrelativistic methods. III. Atomic 4-spinor expansions and integral approximations. *J Chem Phys* 1999, 111:10000.
70. Dyall KG. A systematic sequence of relativistic approximations. *J Comput Chem* 2002, 23:786.
71. Wolf M, Reiher M, Hess BA. The generalized Douglas-Kroll transformation. *J Chem Phys* 2002, 117:9215.
72. Wolf M, Reiher M, Hess BA. Correlated ab initio calculations of spectroscopic parameters of SnO within the framework of the higher-order generalized Douglas-Kroll transformation. *J Chem Phys* 2004, 120.
73. Reiher M, Wolf A. Exact decoupling of the Dirac Hamiltonian. I. General theory. *J Chem Phys* 2004, 121:2037.
74. Reiher M, Wolf A. Exact decoupling of the Dirac Hamiltonian. II. The generalized Douglas-Kroll-Hess transformation up to arbitrary order. *J Chem Phys* 2004, 121:10945.
75. Seino J, Uesugi W, Haeda M. Expectation values in two-component theories. *J Chem Phys* 2010, 132:164108.
76. Kutzelnigg W, Liu W. Quasirelativistic theory equivalent to fully relativistic theory. *J Chem Phys* 2005, 123:241102.
77. Kutzelnigg W, Liu W. Quasirelativistic theory. I. Theory in terms of a quasi-relativistic operator. *Mol Phys* 2006, 104:2225.
78. Liu W, Peng D. Exact two-component Hamiltonians revisited. *J Chem Phys* 2009, 131:031104.
79. Barysz M, Sadlej AJ, Snijders JG. Nonsingular two/one-component relativistic Hamiltonians accurate through arbitrary high order in α^2. *Int J Quantum Chem* 1997, 65:225.
80. Barysz M, Sadlej AJ. Infinite-order two-component theory for relativistic quantum chemistry. *J Chem Phys* 2002, 116:2696.
81. Kedziera D, Barysz M. Spin-orbit interactions and supersymmetry in two-component relativistic methods. *Chem Phys Lett* 2004, 393:521.
82. Kedziera D. Convergence of approximate two-component Hamiltonians: How far is the Dirac limit. *J Chem Phys* 2005, 123:074109.
83. Kedziera D, Barysz M. Non-iterative approach to the infinite-order two-component (IOTC) relativistic theory and the non-symmetric algebraic Riccati equation. *Chem Phys Lett* 2007, 446:176.
84. Iliaš M, Jensen HJA, Roos BO, Urban M. Theoretical study of PbO and the PbO anion. *Chem Phys Lett* 2005, 408:210.
85. Iliaš M, Saue T. An infinite-order two-component relativistic Hamiltonian by a simple one-step transformation. *J Chem Phys* 2007, 126:064102.
86. Barysz M, Mentel L, Leszczynski J. Recovering four-component solutions by the inverse transformation of the infinite-order two-component wave functions. *J Chem Phys* 2009, 130:164114.
87. Filatov M. Comment on 'Quasirelativistic theory equivalent to fully relativistic theory'. J Chem Phys 123, 241102 (2005). *J Chem Phys* 2006, 125:107101.
88. Filatov M, Dyall KG. On convergence of the normalized elimination of the small component (NESC) method. *Theor Chem Acc* 2007, 117:333.
89. Kutzelnigg W, Liu W. Response to Comment on 'Quasirelativistic theory equivalent to fully relativistic theory' J Chem Phys 123, 241102 (2005). *J Chem Phys* 2006, 125:107102.
90. Filatov M, Cremer D. A variationally stable quasi-relativistic method: low-order approximation to the normalized elimination of the small component using an effective potential. *Theor Chem Acc* 2002, 108:168.
91. Filatov M, Cremer D. A new quasi-relativistic approach for density functional theory based on the normalized elimination of the small component. *Chem Phys Lett* 2002, 351:259.
92. Zou W, Filatov M, Cremer D. Development and application of the analytical energy gradient for

the normalized elimination of the small component method. *J Chem Phys* 2011, 134:244117.

93. Zou W, Filatov M, Atwood D, Cremer D. Removal of mercury from the environment—a quantum chemical study with the normalized elimination of the small component (NESC) method. *Inorg Chem* 2013, 52:2497.
94. Kraka E, Zou W, Freindorf M, Cremer D. Energetics and mechanism of the hydrogenation of XH_n for group IV to group VII elements X. *J Chem Theory Comput* 2012, 8:4931.
95. Zou W, Filatov M, Cremer D. Analytic calculation of second-order electric response properties with the normalized elimination of the small component (NESC) method. *J Chem Phys* 2012, 137:084108.
96. Filatov M, Zou W, Cremer D. Relativistically corrected electric field gradients calculated with the normalized elimination of the small component formalism. *J Chem Phys* 2012, 137:054113.
97. Filatov M, Zou W, Cremer D. Analytic calculation of isotropic hyperfine structure constant using the normalized elimination of the small component formalism. *J Phys Chem A* 2012, 116:3481.
98. Filatov M, Zou W, Cremer D. Analytic calculation of contact densities and Mössbauer isomer shifts using the normalized elimination of the small component formalism. *J Chem Theory Comput* 2012, 8:875.
99. Zou W, Filatov M, Cremer D. Development, implementation, and application of an analytic second derivative formalism for the normalized elimination of the small component method. *J Chem Theory Comput* 2012, 8:2617.
100. Cheng L, Gauss J. Analytic energy gradients for the spin-free exact two-component theory using an exact block diagonalization for the one-electron Dirac Hamiltonian. *J Chem Phys* 2011, 135:084114.
101. Cheng L, Gauss J. Analytic second derivatives for the spin-free exact two-component theory. *J Chem Phys* 2011, 135:244104.
102. Cheng L, Gauss J, Stanton JF. Treatment of scalar-relativistic effects on nuclear magnetic shieldings using a spin-free exact-two-component approach. *J Chem Phys* 2013, 139:054105.
103. Filatov M, Zou W, Cremer D. Spin-orbit coupling calculations with the two-component normalized elimination of the small component method. *J Chem Phys* 2013, 139:014106.
104. Kutzelnigg W. Basis set expansion of the Dirac operator without variational collapse. *Int J Quantum Chem* 1984, 25:107.
105. Dyall K. An exact separation of the spin-free and spin-dependent terms of the Dirac-Coulomb-Breit Hamiltonian. *J Chem Phys* 1994, 100:2118.
106. Lancaster P, Rodman L. *Algebraic Riccati Equations*. Oxford: Oxford University Press; 1995.
107. Dyall KG. Interfacing relativistic and nonrelativistic methods. IV. One- and two-electron scalar approximations. *J Chem Phys* 2001, 115:9136.
108. Visscher L, Visser O, Aerts PJC, Nieuwpoort WC. Kinetic balance in contracted basis sets for relativistic calculations. *Int J Quantum Chem Quantum Chem Symp* 1991, 25:131.
109. Andrea D. In: Schwerdtfeger P, ed. *Relativistic Electronic Structure Theory, Volume 11, Part 1. Fundamentals*. Amsterdam: Elsevier; 2002, 203–258.
110. Visser O, Aerts PJC, Hegarty D, Nieuwpoort WC. The use of Gaussian nuclear charge distributions for the calculation of relativistic electronic wavefunctions using basis set expansions. *Chem Phys Lett* 1987, 134:34.
111. Visscher L, Dyall KG. Dirac-Fock atomic electronic structure calculations using different nuclear charge distributions. *At. Data Nuc. Data Tables* 1997, 67:207.
112. Zemach A. Proton structure and the hyperfine shift in hydrogen. *Phys Rev* 1956, 104:1771.
113. Yamaguchi Y, Goddard JD, Osamura Y, Schaefer HFS. *A New Dimension to Quantum Chemistry: Analytic Derivative Methods in Ab Initio Molecular Electronic Structure Theory*. Oxford: Oxford University Press; 1994.
114. Pulay P. Ab initio calculation of force constants and equilibrium geometries. I. Theory. *Mol Phys* 1969, 17:197.
115. Filatov M, Cremer D. Calculation of indirect nuclear spin-spin coupling constants within the regular approximation for relativistic effects. *J Chem Phys* 2004, 120:11407.
116. Herzberg G, Huber K-P. *Molecular Spectra and Molecular Structure*, vol. IV. New York: Van Nostrand; 1979.
117. Shepler C, Balabanov NB, Peterson KA. Ab initio thermochemistry involving heavy atoms: an investigation of the reactions Hg + Ix (X = I, Br, Cl, O). *J Phys Chem A* 2005, 109:10363.
118. Rai AK, Rai SB, Rai DK. Spectral study of the D-X system of the diatomic mercury chloride molecule. *J Phys B At Mol Phys* 1982, 15:3239.
119. Tellinghuisen J, Tellinghuisen PC, Davies SA, Berwanger P, Viswanathan KS. B – X transitions in HgCl and HgI. *Appl Phys Lett* 1982, 41:789.
120. Wilcomb E, Bernstein RB. Dissociation energies of ground-state HgX molecules (X = I, Br, Cl) from analysis of vibrational level spacings. *J Mol Spectrosc* 1976, 62:442.
121. Ullas G, Rai SB, Rai DK. Two-photon optogalvanic spectrum of the C–X system of HgBr. *J Phys B At Mol Phys* 1992, 25:4497.
122. Tellinghuisen J, Ashmore JG. The B – X transition in $^{200}Hg^{79}Br$. *Appl Phys Lett* 1982, 40:867.

123. Tellinghuisen J, Ashmore JG. Mixed representations for diatomic spectroscopic data: application to HgBr. *Chem Phys Lett* 1983, 102:10.

124. Salter PC, Ashmore JG, Tellinghuisen J. The emission spectrum of $^{200}Hg^{127}I$. *J Mol Spectrosc* 1986, 120:334.

125. Filatov M, Cremer D. Relativistically corrected hyperfine structure constants calculated with the regular approximation applied to correlation corrected ab initio theory. *J Chem Phys* 2004, 121:5618.

126. Hellmann H. *Einführung in die Quantenchemie*. Leipzig: F. Deuticke; 1937.

127. Feynman RP. Forces in molecules. *Phys Rev* 1939, 56:340.

128. Goll E, Stoll H, Tierfelder C, Schwerdtfeger P. *Improved dipole moments by combining short-range gradient-corrected density-functional theory with long-range wave-function methods*. *Phys Rev A* 2007, 76:032507.

129. Okabayashi T, Nakaoka Y, Yamazaki E, Tanimoto M. Millimeter- and submillimeter-wave spectroscopy of auf in the ground $X^1\sigma^+$ state. *Chem Phys Lett* 2002, 366:406.

130. Steimle TC, Zhang R, Qin C, Varberg TD. Molecular-beam optical Stark and Zeeman study of the $[17.8]0^+$-$X^1\sigma^+$ (0,0) band system of AuF. *J Phys Chem A* 2013, 117:11737.

131. Reynard LM, Evans CJ, Gerry MCL. The pure rotational spectrum of AuI. *J Mol Spectrosc* 2001, 205:344.

132. Pyykkö P, Xiong X-G, Li J. Aurophilic attractions between a closed-shell molecule and a gold cluster. *Faraday Discuss* 2011, 152:169.

133. Dufayard J, Majournat B, Nedelec O. Predissociation of HgH $A^2\pi_{1/2}$ by inner crossing with $X^2\sigma^+$. *Chem Phys* 1988, 128:537.

134. Nedelec O, Majournat B, Dufayard J. Configuration mixings and line intensities in cdh and HgH $A^2\pi$–$x^2\sigma^+$ transitions. *Chem Phys* 1989, 134:137.

135. Abragam A, Bleaney B. *Electron Paramagnetic Resonance of Transition Ions*. Oxford: Clarendon Press; 1970.

136. Weil JA, Bolton JR. *Electron Paramagnetic Resonance: Elementary Theory and Practical Applications*. Hoboken, NJ: John Wiley & Sons, Inc.; 2007.

137. Belanzoni P, Van Lenthe E, Baerends E-J. An evaluation of the density functional approach in the zero order regular approximation for relativistic effects: magnetic interactions in small metal compounds. *J Chem Phys* 2001, 114:4421.

138. Malkin E, Repiský M, Komorovský S, Mach P, Malkina OL, Malkin VG. Effects of finite size nuclei in relativistic four-component calculations of hyperfine structure. *J Chem Phys* 2011, 134:044111.

139. Stowe AC, Knight LB Jr. Electron spin resonance studies of ^{199}HgH, ^{201}HgH, ^{199}HgD, and ^{201}HgD isolated in neon and argon matrices at 4 K: an electronic structure investigation. *Mol Phys* 2002, 100:353.

140. Knight LB Jr, Fisher TA, Wise MB. Photolytic codeposition generation of the HgF radical in an argon matrix at 12 K: an ESR investigation. *J Chem Phys* 1981, 74:6009.

141. Knight LB Jr, Lin KC. ESR spectroscopy and chemical bonding in CdCN and HgCN molecules. *J Chem Phys* 1972, 56:6044.

142. Karakyriakos E, McKinley AJ. Matrix isolated $HgCH_3$ radical: an ESR investigation. *J Phys Chem A* 2004, 108:4619.

143. Weltner W Jr. *Magnetic Atoms and Molecules*. New York: Van Nostrand Reinhold; 1983.

144. Lucken EAC. *Nuclear Quadrupole Coupling Constants*. London: Academic Press; 1969.

145. Gütlich P, Bill E, Trautwein A. *Mössbauer Spectroscopy and Transition Metal Chemistry: Fundamentals and Applications*. Heidelberg: Springer; 2011.

146. Lucken EAC. In: Smith JAS, ed. *Advances in Nuclear Quadrupole Resonance*, vol. 5. New York: John Wiley; 1983, 86.

147. Parish RV. *NMR, NQR, EPR, and Mössbauer Spectroscopy in Inorganic Chemistry*. Ellis Horwood series in inorganic chemistry. Chichester: E. Horwood; 1990.

148. Haas H, Shirley DA. Nuclear quadrupole interaction studies by perturbed angular correlations. *J Chem Phys* 1973, 58:3339.

149. Neese F. In: Gilbert BC, Davies MJ, Murphy DM, eds. *Electron Paramagnetic Resonance*, vol. 20. Cambridge: The Royal Society of Chemistry; 2007, 73–95.

150. Pernpointner M, Schwerdtfeger P, Hess BA. Accurate electric field gradients for the coinage metal chlorides using the PCNQM method. *Int J Quantum Chem* 2000, 76:371.

151. Arcisauskaite V, Knecht S, Sauer SPA, Hemmingsen L. Fully relativistic coupled cluster and DFT study of electric field gradients at Hg in ^{199}Hg compounds. *Phys Chem Chem Phys* 2012, 14:2651.

152. Kaufmann EN, Vianden RJ. The electric field gradient in noncubic metals. *Rev Mod Phys* 1979, 51:161.

153. Cremer D, Krüger F. Electrlc fieid gradients and nuclear quadrupole coupling constants of isonitriles obtained from Møller-Plesset and quadratic configuration interaction calculations. *J Phys Chem* 1991, 96:3239.

154. Mastalerz R, Barone G, Lindh R, Reiher M. Analytic high-order Douglas-Kroll-Hess electric field gradients. *J Chem Phys* 2007, 127:074105.

155. Pyykkö P. Effect of nuclear volume on nuclear quadrupole coupling in molecules. *Chem Phys Lett* 1970, 6:479.

156. Filatov M, Zou W, Cremer D. On the isotope anomaly of nuclear quadrupole coupling in molecules. *J Chem Phys* 2012, 137:131102.

157. Mössbauer RL. Kernresonanzfluoreszenz von Gammastrahlung in Ir^{191}. *Z Phys* 1958, 151:124.

158. DeBenedetti S, Lang G, Ingalls R. Electric quadrupole splitting and the nuclear volume effect in the ions of Fe^{57}. *Phys Rev Lett* 1961, 6:60.

159. Shirley DA. Application and interpretation of isomer shifts. *Rev Mod Phys* 1964, 36:339.

160. Filatov M. First principles calculation of Mössbauer isomer shift. *Coord Chem Rev* 2009, 253:594.

161. Tucek J, Miglierini M, eds. *Mössbauer Spectroscopy in Materials Science*. Melville, NY: American Inst. of Physics; 2010.

162. Dyar MD, Argesti DG, Schaefer MW, Grant CA, Sklute E. Mössbauer spectroscopy of earth and planetary materials. *Annu Rev Earth Planet Sci* 2006, 34:83.

163. Münck E, Stubna A. In: McCleverty JA, Meyer TB, Lever ABP, eds. *Comprehensive Coordination Chemistry II, Fundamentals: Physical Methods, Theoretical analysis and Case Studies*, vol. 2. New York: Elsevier; 2003, 279–286.

164. Filatov M. On the calculation of Mössbauer isomer shift. *J Chem Phys* 2007, 127:084101.

165. Wilson EB, Decius JC, Cross PC. *Molecular Vibrations. The Theory of Infrared and Raman Vibrational Spectra*. New York: McGraw-Hill; 1955.

166. Visscher L, Saue T, Oddershede J. The 4-component random phase approximation method applied to the calculation of frequency-dependent dipole polarizabilities. *Chem Phys Lett* 1997, 274:181.

167. Norman P, Schimmelpfennig B, Ruud K, Jensen HJA, Ågren H. Relativistic effects on linear and nonlinear polarizabilities studied by effective-core potential, Douglas-Kroll, and Dirac-Hartree-Fock response theory. *J Chem Phys* 2002, 116:6914.

168. Pecul M, Rizzo A. Relativistic effects on the electric polarizabilities and their geometric derivatives for hydrogen halides and dihalogens—a Dirac-Hartree-Fock study. *Chem Phys Lett* 2003, 370:578.

169. Schwerdtfeger P. The CTCP table of experimental and calculated static dipole polarizabilities for the electronic ground states of the neutral elements. 2012. Available at: http://ctcp.massey.ac.nz/dipole-polarizabilities and references cited therein.

170. Pople JA, Krishnan R, Schlegel HB, Binkley JS. Derivative studies in Hartree-Fock and Møller-Plesset theories. *Int J Quantum Chem Quantum Chem Symp* 1979, 13:225.

171. G. Zerbi. *Vibrational Intensities in Infrared and Raman Spectroscopy* W. Person and G. Zerbi. Elsevier, Amsterdam (1982), 23 .

172. Andrews L, Wang X. Infrared spectra and structures of the stable CuH_2^-, AgH_2^-, AuH_2^-, and AuH_4^- anions and the AuH_2 molecule. *J Am Chem Soc* 2003, 125:11751.

173. Leary K, Bartlett N. A new oxidation state of gold: the preparation and some properties of $[AuF^6]^-$ salts. *J Chem Soc Chem Commun* 1972, 1972:903.

174. Goncharov V, Heaven MC. Spectroscopy of the ground and low-lying excited states of ThO^+. *J Chem Phys* 2006, 124:064312.

175. Andrews L, Gong Y, Liang B, Jackson VE, Flamerich R, Li S, Dixon DA. Matrix infrared spectra and theoretical studies of thorium oxide species: ThO_x and Th_2O_y. *J Phys Chem A* 2011, 115:14407.

176. Claassen H, Goodman GL, Holloway JH, Selig H. Raman spectra of MoF_6, TcF_6, ReF_6, UF_6, SF_6, SeF_6, and TeF_6 in the vapor state. *J Chem Phys* 1970, 53:341.

177. Person WB, Kim KC, Campbell GM, Dewey HJ. Absolute intensities of infrared-active fundamentals and combination bands of gaseous PuF_6 and NpF_6. *J Chem Phys* 1986, 85:5524.

178. Krebs B, Hasse K-D. Refinements of the crystal structures of $KTcO_4$, $KReO_4$ and OsO_4. the bond lengths in tetrahedral oxoanions and oxides of d^0 transition metals. *Acta Crystallogr B* 1976, 32:1334.

179. Huston L, Claassen HH. Raman spectra and force constants for OsO_4 and XeO_4. *J Chem Phys* 1970, 52:5646.

180. Cremer D, Larsson JA, Kraka E. *Theoretical and Computational Chemistry, Volume 5, Theoretical Organic Chemistry*. C Parkanyi Elsevier, Amsterdam (1998), 259.

181. Boettcher CJE. *Theory of Electric Polarization*. Amsterdam: Elsevier; 1973.

182. Kellö V, Antušel A, Urban M. Quasi-relativistic coupled cluster calculations of electric dipole moments and dipole polarizabilities of GeO, SnO, and PbO. *J Comp Meth Sci Eng* 2004, 4:753.

183. Lide DR. *CRC Handbook of Chemistry and Physics*. 90th ed. Boca Raton, FL: CRC; 2009-2010.

184. Maryott AA, Buckley F. (1953) *U. S. National Bureau of Standards Circular No. 537*.

185. Furlani TR, King HF. Theory of spinorbit coupling. application to singlet-triplet interaction in the trimethylene biradical. *J Chem Phys* 1985, 82:5577.

186. Fedorov DG, Koseki S, Schmidt MW, Gordon MS. Spin-orbit coupling in molecules: chemistry beyond the adiabatic approximation. *Int Rev Phys Chem* 2003, 22:551.

187. Fleig T. Invited review: relativistic wave-function based electron correlation methods. *Chem Phys* 2012, 395:2.

188. Fedorov DG, Gordon MS. A study of the relative importance of one and two-electron contributions to spin-orbit coupling. *J Chem Phys* 2000, 112:5611.

189. King HF, Furlani TR. Computation of one and two electron spin-orbit integrals. *J Comput Chem* 1988, 9:771.

190. Boettger C. Approximate two-electron spin-orbit coupling term for density-functional-theory DFT calculations using the Douglas-Kroll-Hess transformation. *Phys Rev B* 2000, 62:7809.

191. Majumder S, Matveev AV, Rösch N. Spin-orbit interaction in the Douglas-Kroll approach to relativistic density functional theory. *Chem Phys Lett* 2003, 382:186.

192. Peralta JE, Scuseria GE. Relativistic all-electron two-component self-consistent density functional calculations including one-electron scalar and spin-orbit effects. *J Chem Phys* 2004, 120:5875.

193. van Wüllen C, Michauk C. Accurate and efficient treatment of two-electron contributions in quasirelativistic high-order Douglas-Kroll density-functional calculations. *J Chem Phys* 2005, 123: 204113.

194. Seeger R, Pople JA. Self-consistent molecular orbital methods. XVIII. Constraints and stability in Hartree-Fock theory. *J Chem Phys* 1977, 66:–3045.

195. Hammes-Schiffer S, Andersen HC. The advantages of the general Hartree-Fock method for future computer simulation of materials. *J Chem Phys* 1993, 99:1901.

196. Jimez-Hoyos CA, Henderson TM, Scuseria GE. Generalized Hartree-Fock description of molecular dissociation. *J Chem Theory Comput* 2011, 7: 2667.

